

# A SHELL/3D MODELING TECHNIQUE FOR THE ANALYSIS OF DELAMINATED COMPOSITE LAMINATES

Ronald Krueger<sup>1</sup> and T. Kevin O'Brien<sup>2</sup>

<sup>1</sup> National Research Council Research Associate

<sup>2</sup> U.S. Army Research Laboratory, Vehicle Technology Directorate

NASA Langley Research Center

Hampton, VA 23681

## ABSTRACT

A shell/3D modeling technique was developed for which a local three-dimensional solid finite element model is used only in the immediate vicinity of the delamination front. The goal was to combine the accuracy of the full three-dimensional solution with the computational efficiency of a plate or shell finite element model. Multi-point constraints provided a kinematically compatible interface between the local three-dimensional model and the global structural model which has been meshed with plate or shell finite elements. Double Cantilever Beam (DCB), End Notched Flexure (ENF), and Single Leg Bending (SLB) specimens were modeled using the shell/3D technique to study the feasibility for pure mode I (DCB), mode II (ENF) and mixed mode I/II (SLB) cases. Mixed mode strain energy release rate distributions were computed across the width of the specimens using the virtual crack closure technique. Specimens with a unidirectional layup and with a multidirectional layup where the delamination is located between two non-zero degree plies were simulated. For a local three-dimensional model, extending to a minimum of about three specimen thicknesses on either side of the delamination front, the results were in good agreement with mixed mode strain energy release rates obtained from computations where the entire specimen had been modeled with solid elements. For large built-up composite structures modeled with plate elements, the shell/3D modeling technique offers a great potential for reducing the model size, since only a relatively small section in the vicinity of the delamination front needs to be modeled with solid elements.

## KEY WORDS

Composite materials, fracture mechanics, strain energy release rate, finite element analysis, virtual crack closure technique.

## INTRODUCTION

One of the most common failure modes for composite structures is delamination. The remote loadings applied to composite components are typically resolved into interlaminar tension and shear stresses at discontinuities that create mixed-mode I and II delaminations. To characterize the onset and growth of these delaminations the use of fracture mechanics has become common practice over the past two decades [1-3]. The total strain energy release rate,  $G$ , the mode I component due to interlaminar tension,  $G_I$ , the mode II component due to interlaminar sliding shear,  $G_{II}$ , and the mode III component,  $G_{III}$ , due to interlaminar scissoring shear, are calculated from continuum (2D) and solid (3D) finite element analyses using the virtual crack closure technique [4-8]. In order to predict delamination onset or growth, these calculated  $G$  components are compared to interlaminar fracture toughness properties measured over a range from pure mode I loading to pure mode II loading [9-12]. Even though several specimens have been suggested for the measurement of the mode III interlaminar fracture toughness property [13-14], an interaction criterion incorporating the scissoring shear has not yet been established.

Three-dimensional finite element models have been used to study the behavior of specimens used in fracture toughness testing [7,15-17], as well as the behavior of edge delaminations [1,18] and near-surface delaminations in composite laminates [19,20]. Since many layers of brick elements through the thickness are often necessary to model the individual plies, the size of finite element models required for accurate analyses may become prohibitively large. To improve computational efficiency, built-up structures are therefore traditionally modeled and analyzed using plate or shell finite elements. Computed mixed mode strain energy release rate components, however, depend on many variables such as element order and shear deformation assumptions, kinematic constraints in the neighborhood of the delamination front, and continuity of material properties and section stiffness in the vicinity of the debond when delaminations or debonds are modeled with plate or shell finite elements [7,21]. For example, in reference 21, mesh refinement studies showed that computed  $G_I$ ,  $G_{II}$ , and  $G_{III}$  did not converge when the structure above and below the plane of delamination was modeled with plate elements with different section properties (thickness or layup). A comparison of computed mixed mode strain energy release rates obtained from plate models with values computed from three-dimensional models showed differences in results near the free edges of the structure where the stress state is three-dimensional [22]. These

problems may be avoided by using three-dimensional models. Furthermore, three-dimensional analyses are required when matrix cracks and multiple delaminations need to be modeled at different ply interfaces. Three-dimensional analyses become necessary e.g. to analyze the skin/stringer debonding discussed in reference 23, where the failure at the flange tip is inherently three-dimensional as shown in Figure 1. Matrix cracks and delaminations at different ply interfaces need to be modeled with solid elements. Therefore, methods based on three-dimensional modeling to calculate fracture parameters in built-up structures need to be improved.

The overall objective of the current work is to develop a shell/3D modeling technique for which a local solid finite element model is used only in the immediate vicinity of the delamination front and the remainder of the structure is modeled using plate or shell elements. The goal of the shell/3D technique is to combine the computational efficiency of a plate or shell finite element model with the accuracy of the full three-dimensional solution in the areas of interest. Multi-point constraints provide a kinematically compatible interface between the local three-dimensional model and the surrounding global structural model, which can be meshed with plate or shell finite elements. For large composite structures, the shell/3D modeling technique offers great potential for saving modeling and computational effort because only a relatively small section in the vicinity of the delamination front needs to be modeled with solid elements as shown in Figure 2. A significant reduction in model size can be expected compared to a full three-dimensional model.

In the current investigation, the feasibility of the shell/3D technique proposed is studied for the pure mode I case, mode II case and a mixed mode I/II case. This is accomplished by using simple specimens like the double cantilever beam (DCB), end notched flexure (ENF), and single leg bending (SLB) specimens. For each specimen, mixed mode strain energy release rate distributions were computed across the width from nonlinear finite element analyses using the virtual crack closure technique [3-5]. The length of the local three-dimensional model around the delamination front was increased until the results computed were within 1% of mixed mode strain energy release rates obtained from previous analyses where the entire specimen had been modeled with solid elements [24].

## SPECIMEN DESCRIPTION

For this investigation the double cantilever beam (DCB), the end notched flexure (ENF), and the single leg bending (SLB) specimens, as shown in Figure 3, were chosen to study the feasibility of the shell/3D technique for the pure mode I case, mode II case and a mixed mode I/II case, respectively. For specimen preparation and testing procedure the reader is referred to the literature [2, 9, 10, 25]. In general DCB, ENF and mixed mode tests are performed on unidirectionally reinforced laminates, which means that delamination growth occurs at a [0/0] interface and crack propagation is parallel to the fibers. Although this unidirectional layup is desired for standard test methods to characterize fracture toughness, this kind of delamination growth will rarely occur in real structures. Previously, a number of combined experimental and numerical studies on unidirectional and multidirectional laminates have been performed where the critical strain energy release rates of various interfaces were evaluated under mode I, mode II and mixed-mode conditions [15, 16, 17, 26, 27]. Three different laminates were selected from these previous studies. The unidirectional layup  $[0]_{32}$  was designated UD32, the unidirectional layup  $[0]_{24}$  was designated UD24 and the multidirectional layup  $[30/-30/0/-30/0/30/0_4/30/0/-30/0/-30/30/-30/30/0/30/0/-30/0_4/-30/0/30/0/30/-30]$  was designated  $D_{\pm 30}$ . The arrow denotes the location of the delamination, which for all three laminates was located in the midplane. These laminates were selected as experimental and computational results from previous studies were readily available. From all laminates studied the difference in ply orientation at the delaminated interface was maximal for the  $D_{\pm 30}$  layup. It was selected for the current study to demonstrate that the shell/3D technique described can be used independent from laminate layup. In the original studies the  $D_{\pm 30}$  layup was chosen to investigate the influence of stacking sequence on energy release rate distributions in various specimens [16, 17, 26]. For interfacial delaminations between two orthotropic solids care must be exercised in interpreting the computed mixed mode energy release rates obtained from the virtual crack closure technique. This will be discussed in detail in the section on specimens with multidirectional layup. The UD32 and  $D_{\pm 30}$  layup were made of C12K/R6376 graphite/epoxy and the UD24 layup was made of T300/1076 graphite/epoxy. The material properties are given in Table 1 and the layup is summarized in Table 2.

## FINITE ELEMENT ANALYSIS

The goal of this investigation was to study the accuracy of the shell/3D modeling technique by comparing strain energy release rates computed using the shell/3D modeling technique to results obtained from full three-dimensional models. All three specimens were previously modeled entirely with solid elements, and the influence of element selection on computed mixed mode strain energy release rates was studied[24].

A shell/3D model of a typical specimen is shown in Figure 4. For the entire investigation, the ABAQUS® geometric nonlinear analysis procedure was used. This was done in accordance with previous studies which were used as reference solutions. These studies focussed on the influence of stacking sequence on energy release rate distributions in various specimens, which required the consideration of geometric nonlinearity. The global section was modeled with ABAQUS® four-noded S4 type quadrilateral shell elements. The local three-dimensional section was modeled with ABAQUS® solid eight-noded C3D8I type elements. Incompatible mode elements, C3D8I, are recommended for bending and contact problems. In these elements internal deformation modes are added to the standard displacement modes of the element in order to eliminate the parasitic shear stresses that occur in bending [28]. Likewise, elements where a lower-order, reduced, integration is used to form the element stiffness such as the S8R and C3D20R element types usually provide more accurate results in bending and reduce running time. Therefore, a combination of reduced integrated eight-noded quadrilateral shell elements S8R with solid twenty-noded hexahedral elements C3D20R was also studied. The transition from the global shell element model to the local three-dimensional model in the vicinity of the delamination front was accomplished by using multi-point constraint options given by ABAQUS® to enforce appropriate translations and rotations at the shell-solid interface [28]. The theory used for the multi-point constraint option assumes that the interface between the shell elements and solid elements is a surface containing the normals to the shell along the line of intersection of the meshes, so that the lines of nodes on the solid mesh side of the interface in the normal direction to the surface are straight lines. The nodes on the solid mesh side have the possibility of moving along the line and the line is allowed to change length, which means that there are no constraints in thickness direction [28]. An improved coupling of the shell element model to the local three-dimensional model may be obtained by the use of special transition elements using formulations for the shell/3D transition based on a higher-order shell theory [29]. Interpenetration of the delaminated faces was prevented by using multi point constraints [28]. The loading for each specimens was applied as a distributed load as shown in Figure 3.

The specimens with unidirectional layup were modeled by six elements through the specimen thickness as shown in the detail of Figure 4(a). For the specimens with D±30 layup, two plies on each side of the delamination were modeled individually using one element for each ply as

shown in Figure 4(b). The adjacent four plies were modeled by one element with material properties smeared using the rule of mixtures [30]. This procedure used did not ensure the full A-B-D contribution of the plies, however, appeared suitable to enforce a reasonable model size. The adjacent element extended over the four  $0^\circ$  plies. The six outermost plies were modeled by one element, again with smeared material properties. The delamination was modeled as a discrete discontinuity in the center of the specimen, with separate, unconnected nodes (with identical coordinates) on the upper and lower surfaces of the delaminated section. Referring to Figure 4, the specimens were divided into a center section of width,  $f$ , and a refined edge section,  $e$ , to capture local edge effects and steep gradients. These sections appear as dark areas in the full view of the specimen. Along the length of the model, a refined mesh of length,  $c$ , was used in the vicinity of the delamination front as shown in Figure 4. The influence of the mesh size around the delamination front on computed mixed mode strain energy release rates was previously studied using full three-dimensional models [24].

Along the length of the model a refined mesh of length  $c=5$  mm with  $n=10$  elements was used for the UD24 layup,  $c= 3.0$  mm, 12 elements for the  $D\pm 30$  layup, and  $c= 6.0$  mm,  $n=24$  elements was used for the UD32 layup in the vicinity of the delamination front. These section lengths,  $c$ , had been selected in previous studies [27] and remained unchanged during the current investigations. To study the influence of the size of the local zone on computed mixed mode strain energy release rates, the total length of the local zone modeled with solid elements,  $d$ , was varied between 10 to 30 mm, in 5mm increments.

The Virtual Crack Closure Technique (VCCT) was used to calculate strain energy release rates [3-5]. Nodal point forces computed at the delamination front were multiplied with the relative delamination opening at nodal points one element behind the front to obtain the energy required to virtually close the delamination in one simple step. The energy is divided by the crack surface area virtually closed to obtain the strain energy release rate. The mode I, mode II and mode III components of the strain energy release rate,  $G_I$ ,  $G_{II}$  and  $G_{III}$ , were calculated for eight noded elements as given in reference [5]. For the twenty noded solid elements the equations to calculate the strain energy release rate components at the element corner nodes and at the mid side node were taken from reference 19. Additional information with respect to the application of the VCCT and improved equations for twenty noded solids are given in the literature [4-8, 19, 24]. The data required to perform the Virtual Crack Closure Technique were accessed from the ABAQUS<sup>®</sup> result file. The calculations were performed in a separate post processing step using nodal displacements and nodal forces obtained from elements at the delamination front.

## ANALYSIS OF SPECIMENS WITH UNIDIRECTIONAL LAYUP

Numerical validation of the shell/3D modeling technique was performed first using models of unidirectionally laminated DCB, ENF and SLB specimens in order to study the pure mode I case, mode II case and a mixed mode I/II case. For each specimen, mixed mode strain energy release rate distributions were computed across the width from nonlinear finite element analyses using the virtual crack closure technique. Results were compared to mixed mode strain energy release rates obtained from previous analyses where the entire specimen had been modeled with solid elements [24].

### COMPUTATION OF STRAIN ENERGY RELEASE RATES ACROSS A STRAIGHT DELAMINATION FRONT IN A DCB SPECIMEN WITH UNIDIRECTIONAL LAYUP

A shell/3D model of a DCB specimen made of unidirectional layup UD24 is shown in Figure 4(a). The global section was modeled with S8R type shell elements. The local three-dimensional section was modeled with solid C3D20R type elements. A combination of quadrilateral shell elements S4 with solid eight-noded elements C3D8I, was also studied. Along the length a refined mesh of length  $c=5$  mm with 10 elements was used in the vicinity of the delamination front. This section length,  $c$ , was kept constant during the entire investigation. To study the influence of the length of the local zone on computed mixed mode strain energy release rates, the total length of the local zone modeled with solid elements,  $d$ , was varied ( $d=10, 15, 20, 25, 30$  mm) as shown in Figures 4 and 5 (a) to (e).

The computed strain energy release rate distributions across the width of the specimen are shown in Figure 6 for the combination of twenty noded brick elements in the local three-dimensional model with eight noded shell elements in the global model. In Figure 6 the computed mode I strain energy release rate normalized with respect to the value from beam theory,

$$G_{I,beam}(a) = \frac{12 a^2 P^2}{B^2 h^3 E_1}$$

is plotted versus the normalized width,  $y/B$ , of the specimen. Here,  $a$  denotes the delamination length,  $P$  the external load,  $B$  the specimen width,  $h$  the thickness of the cantilever arms as shown in Figure 3 and  $E_1$  the modulus of elasticity. The mode I strain energy release rate is fairly constant in the center part of the specimen progressively dropping towards the edges causing the straight front to grow into a curved front as explained in detail in the literature [8, 15, 31, 32]. As expected, the mode II and mode III strain energy release rates are computed to be nearly zero and hence are not shown. With increasing length of the local three-dimensional model,  $d$ , computed results from the shell/3D model converge. For a local three-dimensional model extending to a minimum of about

three specimen thicknesses in front and behind the delamination front ( $d/2h=6.67$ ), the results were within 1% of the mode I strain energy release rates obtained from computations where the entire specimen had been modeled with solid elements. The shell/3D model is capable of accurately simulating the anticlastic bending effect that causes the strain energy release rate to be highest in the center of the specimen and lowest at its edges. Results for the combination of eight noded brick elements with four noded shell elements are shown in Figure 7. When compared to the model with twenty noded solids and eight noded shell elements, the combination of eight noded brick elements with four noded shell elements yields almost identical results and provides a reduced model size. Therefore, the combination of eight noded brick elements with four noded shell elements was used for the remainder of this study.

#### COMPUTATION OF STRAIN ENERGY RELEASE RATES ACROSS A STRAIGHT DELAMINATION FRONT IN AN ENF SPECIMEN WITH UNIDIRECTIONAL LAYUP

A shell/3D model of an ENF specimen with unidirectional UD24 layup is shown in Figure 8. The global section was modeled with quadrilateral S4 type shell elements. The local three-dimensional section was modeled with eight-noded C3D8I type elements. As discussed in the study of the DCB specimen above, the section length,  $c$ , was kept constant during the entire investigation.

In Figures 9 and 10 the computed mode II and mode III strain energy release rates normalized with the reference value,  $G_{II,beam}$ , from classical beam theory (not accounting for transverse shear)

$$G_{II,beam}(a) = \frac{9 a^2 P^2}{16 B^2 h^3 E_1}$$

are plotted versus the normalized width,  $y/B$ , of the specimen. The mode II strain energy release rate is fairly constant across almost the entire width of the specimen, peaking in the immediate vicinity of the edges. The mode III contribution is zero in the center of the specimen peaking to about only 5% of  $G_{II,beam}$  at the edges. The computed  $G_I$  values are nearly zero and therefore are not shown. With increasing length of the local three-dimensional model,  $d$ , computed results from the shell/3D model converge to the solution obtained from a full three-dimensional model. The results obtained from all shell/3D models are in excellent agreement with the mode III strain energy release rate obtained from computations where the entire specimen had been modeled with solid elements as shown in Figure 10. For a unidirectional layup, however, the mode III contribution is very small. Therefore, the influence of the size of the local three-dimensional model on mode II and mode III separation needs to be verified for a case where the mode III contribution is more obvious and the mode II contribution is less dominant. This will be discussed in the section on the ENF specimen with multidirectional layup.

## COMPUTATION OF STRAIN ENERGY RELEASE RATES ACROSS A STRAIGHT DELAMINATION FRONT IN A SLB SPECIMEN WITH UNIDIRECTIONAL LAYUP

The single leg bending (SLB) specimen, as shown in Figure 3(c), was introduced for the determination of fracture toughness as a function of mixed mode I/II ratio [17, 25]. This test may be performed in a standard three point bending fixture such as that used for the ENF test. By varying the relative thickness of the delaminated regions ( $t_1$  and  $t_2$ ) various mode mixities may be achieved. The test is of particular interest because compliance calibration can be used to accurately determine the critical strain energy release rate [17]. This type of specimen was selected for this study to verify that the shell/3D modeling technique is also capable of accurately simulating the mixed mode I/II case. Mixed mode strain energy release rates which served as reference solutions had been computed in a previous study using three-dimensional FE models [24].

A shell/3D model of a SLB specimen with unidirectional UD32 layup is shown in Figure 11. The global section was modeled with quadrilateral S4 type shell elements. The local three-dimensional section was modeled with eight-noded C3D8I type elements. Along the length a refined mesh of length  $c=6$  mm with 24 elements was used in the vicinity of the delamination front. As discussed in the study of the DCB and ENF specimens above, the section length,  $c$ , was kept constant during the entire investigation and the local zone modeled with solid elements,  $d$ , was varied.

In Figures 12 to 14 the computed mode I, II and mode III strain energy release rates are plotted versus the normalized width,  $y/B$ , of the specimen. As shown in Figure 12, the mode I strain energy release rate is fairly constant in the center part of the specimen progressively dropping towards the edges as previously discussed for the DCB specimen. The mode II strain energy release rate as shown in Figure 13 is fairly constant across almost the entire width of the specimen, peaking in the immediate vicinity of the edges, which was discussed earlier in the section about the ENF specimen. As shown in Figure 14, the mode III contribution is zero in the center of the specimen peaking to about only 8% of  $G_{II}$  at the edges. With increasing length of the local three-dimensional model,  $d$ , computed mode I and II strain energy release rates from the shell/3D model approach the solution obtained from a full three-dimensional model. As shown in Figure 14, the results obtained from all shell/3D models are in excellent agreement with the mode III strain energy release rate obtained from computations where the entire specimen had been modeled with solid elements.

## ANALYSIS OF SPECIMENS WITH A MULTIDIRECTIONAL LAYUP

In general DCB, ENF and mixed mode tests are performed on unidirectionally reinforced laminates, which means that delamination growth occurs at a [0/0] interface and crack propagation is parallel to the fibers. Although this unidirectional layup is desired for standard test methods to characterize fracture toughness, this kind of delamination growth will rarely occur in real structures. Previously, a number of combined experimental and numerical studies on specimens with multidirectional layup have been performed where the critical strain energy release rates of various interfaces were evaluated under mode I, mode II and mixed-mode conditions [16, 17, 27].

In this study, DCB, ENF and SLB specimens with a multidirectional layup were modeled in order to study the pure mode I case, mode II case and a mixed mode I/II case. For each specimen type, mixed mode strain energy release rate distributions were computed across the width from nonlinear finite element analyses using the virtual crack closure technique. Results were compared to mixed mode strain energy release rates obtained from previous analyses where the entire specimen had been modeled with solid elements [24].

Previous investigations have shown that care must be exercised in interpreting the values for  $G_I$ ,  $G_{II}$  and  $G_{III}$  obtained using the virtual crack closure technique for interfacial delaminations between two orthotropic solids [33, 34]. Mathematical solutions of the near crack tip field indicate that stresses start to oscillate in the immediate vicinity of the tip when crack growth occurs at interfaces between materials with dissimilar properties. In the current investigation, this phenomenon has to be considered as the delamination growth occurs at a  $+30^\circ/-30^\circ$  interface. The mixed mode SLB specimen was studied previously to determine an appropriate mesh size for full three-dimensional models [24]. This mesh was used in the current study for the models of the multidirectional DCB and ENF and SLB specimens.

### COMPUTATION OF STRAIN ENERGY RELEASE RATES ACROSS A STRAIGHT DELAMINATION FRONT IN A DCB SPECIMEN

A shell/3D model of a DCB specimen is shown in Figure 15. The global section was modeled with S4 type shell elements. The local three-dimensional section was modeled with C3D8I type solid elements. Along the length a refined mesh of length  $c=3$  mm with 12 elements was used in the vicinity of the delamination front, which is identical to the refined mesh used for the full three-dimensional model from a previous study [24]. This section length,  $c$ , was kept constant during the entire investigation. To study the influence of the length of the local zone on computed mixed mode strain energy release rates, the total length of the local zone modeled with solid elements,  $d$ , was varied ( $d=10, 15, 20, 25, 30$  mm) as shown in Figures 4 and 5(a) to (f). The effect of local penetration of the cantilever arms at the specimen edge near the delamination front on

computed mixed mode strain energy release rates was investigated in a previous study [24]. The results obtained from models including contact were almost in exact agreement with results from simple analyses, where the penetration was not prevented. For the current study it was therefore chosen not to prevent the penetration and thus avoid the complicated contact analysis for the remainder of this study.

The computed strain energy release rate distributions across the normalized width of the specimen are shown in Figure 16. The mode I strain energy release rate is fairly constant in the center part of the specimen progressively dropping towards the edges causing the straight front to grow into a curved front. Basically the distribution is similar to that computed for the UD24-layup. For specimens with multidirectional layup the zone with a constant mode I distribution in the center becomes smaller and the drop towards the edges is more pronounced. This phenomenon can be correlated to the magnitude of a non-dimensional ratio,  $D_c = (D_{12}^2/D_{11}D_{22})$ , of the flexural rigidities in the individual arms of the specimens. The effect of magnitude of the non-dimensional ratio,  $D_c$ , on the distribution of energy release rate across the width of the specimen has been the subject of detailed experimental and analytical investigations [16]. As expected, the mode II and mode III strain energy release rates are computed to be nearly zero and hence are not shown. With increasing length of the local three-dimensional model,  $d$ , computed results from the shell/3D model approach the solution obtained from a full three-dimensional model. For a local three-dimensional model extending to a minimum of about three specimen thicknesses in front and behind the delamination front ( $d/2h=6.16$ ), the results were within 1.5% of the mode I strain energy release rates obtained from computations where the entire specimen had been modeled with solid elements. The good agreement with results obtained from full three-dimensional models suggests that these effects are accurately simulated by the shell/3D model.

#### COMPUTATION OF STRAIN ENERGY RELEASE RATES ACROSS A STRAIGHT DELAMINATION FRONT IN AN ENF SPECIMEN

The mode II strain energy release rate computed for an ENF specimen made of unidirectional layup is fairly constant across almost the entire width of the specimen, peaking in the immediate vicinity of the edges and accompanied by local mode III contributions in the same areas [15]. These peaks become more visible for specimens with multidirectional layup [16, 26, 27]. Therefore an ENF specimen with  $D_{\pm 30}$  layup was selected for this study to verify the accuracy of the shell/3D technique in simulating this local mixed mode case near the edge of the specimen.

A shell/3D model of an ENF specimen is shown in Figure 17. The global section was modeled with quadrilateral S4 type shell elements. The local three-dimensional section was modeled with eight-noded C3D8I type elements. As discussed in the study of the DCB specimen above, the

section length,  $c$ , was kept constant during the entire investigation. Earlier studies [27] showed, that penetration of the arms could be prevented by introducing multi point constraints in the plane of delamination only along a string of nodes above the left support. The use of multi-point constraints appears advantageous as less modeling effort is required and a computationally expensive contact analysis is avoided. The results obtained from models including contact were almost in exact agreement with the values obtained from a contact analysis [24]. Therefore, the technique using the multi point constraints to avoid penetration was used for the remainder of this study.

The computed mode II and III strain energy release rate distributions across the normalized width of the specimen are shown in Figures 18 and 19. The mode II strain energy release rate is fairly constant across almost the entire width of the specimen, peaking near the edges and accompanied by local mode III contributions in the same area. Compared to the UD32 layup, these peaks become more visible for specimens with  $D_{\pm 30}$  layup caused by increased anticlastic bending which can be correlated to the magnitude of the non-dimensional ratio,  $D_c = (D_{12}^2/D_{11}D_{22})$ , discussed earlier. The effect of magnitude of  $D_c$ , on the distribution of energy release rate across the width of the ENF specimen has been the subject of detailed experimental and analytical investigations [16, 26]. As expected, the mode I strain energy release rates is computed to be nearly zero and, hence, is not shown. With increasing length of the local three-dimensional model,  $d$ , computed results from the shell/3D model approach the solution obtained from a full three-dimensional model. The results indicate that the shell/3D technique is capable of accurately simulating the increased anticlastic bending effect.

#### COMPUTATION OF STRAIN ENERGY RELEASE RATES ACROSS A STRAIGHT DELAMINATION FRONT IN A SLB SPECIMEN

A shell/3D model of a SLB  $D_{\pm 30}$  specimen is shown in Figure 20. The global section was modeled with quadrilateral S4 shell elements. The local three-dimensional section was modeled with eight-noded C3D8I type elements. As discussed earlier, the section length,  $c$ , was kept constant during the entire investigation. The effect of local penetration of the cantilever arms at the specimen edge near the delamination front on computed mixed mode strain energy release rates was investigated in a previous study [27]. The results obtained from models including contact were almost in exact agreement with results from simple analyses, where the penetration was not prevented. For the current study it was therefore chosen not to prevent the penetration and thus avoid the complicated contact analysis for the remainder of this study.

The computed mode I, II and III strain energy release rate distributions across the width of the specimen are shown in Figures 21 to 23. The energy release rate distributions become slightly asymmetric compared to the DCB and ENF specimens with  $D_{\pm 30}$  layup and the SLB specimen

with UD32 layup. Bending-twisting coupling in the arms can be ruled out as a possible cause for the asymmetric distribution because extreme care was exercised in designing the  $D_{\pm 30}$  layup so that the non-dimensional ratio  $B_t$  is negligible. The non-dimensional ratio  $B_t = D_{16}/D_{11}$  provides a measure of the amount of bending-twisting coupling that will occur in a given specimen [16]. The energy release rates in the SLB specimen is asymmetric because only one of the delaminated regions is loaded. Higher energy release rates are computed at the edge, to which the local orientation of the fibers provides a natural load path. At the other edge the local load path is very compliant and the energy release rate values are smaller [17]. Similar observations were made for a through the width delamination in a  $-45/90$  interface of a tensile test specimen [18]. The observed pronounced drop in  $G_I$  towards the edges is caused by increased anticlastic bending which can be correlated to the magnitude of the non-dimensional ratio,  $D_c = (D_{12}^2/D_{11}D_{22})$ , discussed earlier. The mode II distributions as shown in Figures 22 is fairly constant across almost the entire width of the specimen and peaks near the edges accompanied by a local mode III contribution. Compared to the UD32 layup these peaks become more visible for specimens with the  $D_{\pm 30}$  layup. For the  $D_{\pm 30}$  layup also a considerable amount of mode III is present as shown in Figure 23. The effect of magnitude of  $D_c$ , on the distribution of energy release rate across the width of the SLB specimen has been the subject of detailed experimental and analytical investigations [17]. With increasing length of the local three-dimensional model,  $d$ , computed results from the shell/3D model approach the solution obtained from a full three-dimensional model. These results indicate that the shell/3D technique is capable of accurately simulating the increased anticlastic bending which causes the mode II and III strain energy release rate to be higher towards the free edges.

## CONCLUDING REMARKS

A shell/3D modeling technique was presented for the analysis of composite laminates with delaminations. The individual mode and total strain energy release rates along the delamination front were evaluated. In this analysis a local solid finite element model was used only in the immediate vicinity of the delamination front. The goal was to combine the accuracy of the full three-dimensional solution with the computational efficiency of the plate or shell finite element model. Multi-point constraints provided a kinematically compatible interface between the local three-dimensional model and the global structural model which was meshed with shell finite elements.

For DCB, ENF, and SLB specimens, mixed mode strain energy release rate distributions were computed across the width from geometrically nonlinear finite element analyses using the virtual crack closure technique. These computations were used to study the feasibility of the proposed shell/3D modeling technique for the pure mode I case (DCB), mode II case (ENF) and a mixed mode I/II case (SLB). Specimens with a unidirectional layup as well as a multidirectional

layup were simulated. For each specimen, mixed mode strain energy release rate distributions were computed across the width from nonlinear finite element analyses using the virtual crack closure technique and compared to reference solutions obtained from geometrically nonlinear full three-dimensional models.

For the current investigation, two shell/3D combinations were studied: eight noded solid elements in the local section combined with four noded shell elements in the global section of the model and twenty-noded solid elements in the local section combined with eight-noded shell elements in the global section. The shell elements were connected to the local three-dimensional model using multi-point constraints to enforce appropriate translations and rotations.

Finite element analyses showed that the accuracy achieved depends on the size of the local three-dimensional model around the delamination front. With increasing length of the local three-dimensional model, the computed results approached the strain energy release rates obtained from full three-dimensional finite element analysis for all specimens, layups and element types. The results were in good agreement with the reference solution once the local zone was extended in front and behind the delamination front to about three times the specimen thickness.

For large composite structures, the shell/3D modeling technique offers great potential for reducing the model size because only a relatively small section in the vicinity of the delamination front needs to be modeled with solid elements. A significant reduction in model size can be expected compared to a full three-dimensional model. In the current investigation, the application of the shell/3D technique reduced the number of degrees of freedom by about 35% compared to a full three-dimensional model for all three specimen types. Existing plate models may be modified to shell/3D models, which is a considerable advantage compared to the creation of an entirely new three-dimensional finite element model.

## REFERENCES

- [1] O'Brien, T.K., "Characterization of Delamination Onset and Growth in a Composite Laminate," *Damage in Composite Materials, ASTM STP 775*, 1982, pp. 140-167.
- [2] O'Brien, T.K. "Interlaminar fracture toughness: the long and winding road to standardization," *Composites Part B*, Vol. 29B, 1998, pp. 57-62.
- [3] Martin, R. H., "Incorporating Interlaminar Fracture Mechanics Into Design," International Conference on Designing Cost-Effective Composites, IMechE Conference Transactions, London, 15-16 September, 1998, pp. 83-92.
- [4] Rybicki, E.F. and Kanninen, M.F., "A Finite Element Calculation of Stress Intensity Factors by a Modified Crack Closure Integral," *Eng. Fracture Mech.*, 9, 1977, pp. 931-938.
- [5] Raju, I.S., "Calculation Of Strain-Energy Release Rates With Higher Order And Singular Finite Elements," *Eng. Fracture Mech.*, 28, 1987, pp. 251-274.
- [6] Buchholz, F.G., Grebner, H., Dreyer, K.H. and Krome, H., "2D- and 3D-Applications of the Improved and Generalized Modified Crack Closure Integral Method," *Computational Mechanics '88*, Atluri, S.N. and Yagawa, G., eds., Springer Verlag, 1988.
- [7] Raju, I.S., Sistla, R. and Krishnamurthy, T., "Fracture Mechanics Analysis For Skin-Stiffener Debonding," *Eng. Fracture Mech.*, 54, 1996, pp. 371-385.
- [8] Raju, I.S., Shivakumar, K.N. and Crews, J.H., "Three-dimensional elastic analysis of a composite double cantilever beam specimen," *AIAA J.*, 26, 1988, pp. 1493-1498.
- [9] O'Brien, T.K. and Martin, R.H., "Round Robin Testing for Mode I Interlaminar Fracture Toughness of Composite Materials," *J. of Composite Technology and Research.*, 1993, pp. 269-281.
- [10] O'Brien, T.K. "Composite Interlaminar Shear Fracture Toughness,  $G_{IIc}$ : Shear Measurement or Shear Myth ?," *Composite Materials: Fatigue and Fracture, Seventh Volume, ASTM STP 1330*, 1998, pp. 3-18.
- [11] Reeder, J.R and Crews, J.H., "Redesign of the Mixed-Mode Bending Delamination Test to Reduce Nonlinear Effects," *J. of Composite Technology and Research.*, 1992, pp. 12-19.
- [12] Reeder, J.R., "A Bilinear Failure Criterion for Mixed-Mode Delamination," *Composite Materials: Testing and Design, Eleventh Volume, ASTM STP 1206*, 1993, pp. 303-322.
- [13] Robinson, P. and Song, D.Q., "A new Mode III delamination test for composites," *Advanced Composites Letters*, 1992,5(1), pp. 160-164.
- [14] Lee, S.M., "An Edge Crack Torsion Method for Mode III Delamination Fracture Testing," *J. of Composite Technology and Research*, 1993, pp. 193-201.
- [15] Krüger, R., König, M. and Schneider, T., "Computation of Local Energy Release Rates Along Straight and Curved Delamination Fronts of Unidirectionally Laminated DCB- and ENF - Specimens," AIAA-93-1457-CP, *Proc. 34th AIAA/ASME/ASCE/AHS/ASC SSDM*

- Conference, La Jolla, CA, 1993, pp. 1332-1342.*
- [16] Davidson, B.D., Krüger, R. and König, M., "Effect of Stacking Sequence on Energy Release Rate Distributions in Multidirectional DCB and ENF specimens," *Engineering Fracture Mechanics*, 1996, 55(4), pp. 557-569.
  - [17] Davidson, B.D., Krüger, R. and König, M., "Three Dimensional Analysis of Center Delaminated Unidirectional and Multidirectional Single Leg Bending Specimens," *Composites Science and Technology*, 1995, 54(4), pp. 385-394.
  - [18] Salpekar, S.A. and O'Brien, T.K., "Combined Effect of Matrix Cracking and Free Edge on Delamination," *Composite Materials: Fatigue and Fracture, Third Volume, ASTM STP 1110*, 1991, pp. 287-311.
  - [19] Whitcomb, J.D., "Three-Dimensional Analysis of a Postbuckled Embedded Delamination," *J. Composite Mat.*, Vol. 23, 1989, pp. 862-889.
  - [20] Krüger, R., Rinderknecht, S., Hänsel, C., and König, M., "Computational Structural Analysis and Testing: An Approach to Understand Delamination Growth," *Fracture of Composites*, E.A. Armanios, ed., Key Eng. Mat., Vols. 120-121, Transtec Publ. Ltd., 1996, pp. 181-202.
  - [21] Glaessgen, E.H., Riddell, W.T., and Raju, I.S., "Effect of Shear Deformation and Continuity on Delamination Modeling with Plate Elements," *Proceedings of the AIAA/ASME/ASCE/AHS/ASC 39th Structures, Structural Dynamics and Materials Conference*, AIAA-98-2023-CP, 1998.
  - [22] Krüger, R., Rinderknecht, S., and König, M., "Two- and Three-Dimensional Finite Element Analyses of Crack Fronts in a Multidirectional Composite ENF Specimen," ISD-Report No. 97/1, Institute for Statics and Dynamics of Aerospace Structures, University of Stuttgart, 1997.
  - [23] Krueger, R., Cvitkovich, M.K., O'Brien, T.K. and Minguet, P.J., "Testing and Analysis of Composite Skin/Stringer Debonding Under Multi-Axial Loading," NASA TM-1999-209097, February 1999.
  - [24] Krueger, R., and O'Brien, T.K., "A Shell/3D Modeling Technique for the analysis of delaminated composite laminates," NASA/TM-2000-210287, ARL-TR-2207, June 2000.
  - [25] Davidson, B.D. and Sundararaman, V., "A single leg bending test for interfacial fracture toughness determination," *Int. J. of Fracture*, Vol. 78, 1996, pp. 193-210.
  - [26] Davidson, B.D., Krüger, R. and König, M., "Three Dimensional Analysis and Resulting Design Recommendations for Unidirectional and Multidirectional End-Notched Flexure Tests", *J. Compos. Mater.*, Vol. 29, 1995, pp. 2108-2133.
  - [27] Krüger, R., "Three Dimensional Finite Element Analysis of Multidirectional Composite DCB, SLB and ENF Specimens," ISD-Report No. 94/2, Institute for Statics and Dynamics of Aerospace Structures, University of Stuttgart, 1994.

- [28] ABAQUS/Standard, "User's Manual, Volume II," Version 5.6, 1996.
- [29] Dávila, C. G., "Solid-To-Shell Transition Elements for the Computation of Interlaminar Stresses", *Computing Systems in Engineering*, Vol. 5, No. 2, 1994, pp. 193-202.
- [30] Tsai, S.W., *Theory of Composite Design*, Think Composites, ISBN 0-9618090-3-5, pp. 4-6,7-3, 1992.
- [31] Crews, J. H., Shivakumar, K. N., and Raju, I. S., "Strain energy release rate distribution for double cantilever beam specimens," *AIAA J.*, Vol. 29, 1991, pp. 1686-1691.
- [32] Davidson, B. D., "An analytical investigation of delamination front curvature in double cantilever beam specimens," *J. Compos. Mater.*, Vol. 24, 1990, pp. 1124-1137.
- [33] Raju, I. S., Crews, J.H., and Aminpour, M.A., "Convergence of Strain Energy Release Rate Components for Edge-Delaminated Composite Laminates," *Eng. Fracture Mech.*, 30, 1988, pp. 383-396.
- [34] Sun, C. T. and Manoharan, M. G., "Strain Energy Release Rates of an Interfacial Crack Between Two Orthotropic Solids," *J. Compos. Mater.*, Vol. 23, May 1989, pp. 460-478.

## TABLES

TABLE 1. MATERIAL PROPERTIES.

T300/1076 Unidirectional Graphite/Epoxy Prepreg [16]		
$E_{11} = 139.4$ GPa	$E_{22} = 10.16$ GPa	$E_{33} = 10.16$ GPa
$\nu_{12} = 0.30$	$\nu_{13} = 0.30$	$\nu_{23} = 0.436$
$G_{12} = 4.6$ GPa	$G_{13} = 4.6$ GPa	$G_{23} = 3.54$ GPa
C12K/R6376 Unidirectional Graphite/Epoxy Prepreg [16]		
$E_{11} = 146.9$ GPa	$E_{22} = 10.6$ GPa	$E_{33} = 10.6$ GPa
$\nu_{12} = 0.33$	$\nu_{13} = 0.33$	$\nu_{23} = 0.33$
$G_{12} = 5.45$ GPa	$G_{13} = 5.45$ GPa	$G_{23} = 3.99$ GPa

TABLE 2. STACKING SEQUENCE.

Layup-ID	Stacking Sequence	Material
UD24	$[0]_{24}$	T300/1076
UD32	$[0]_{32}$	C12K/R6376
D $\pm$ 30	$[30/-30/0/-30/0/30/0_4/30/0/-30/0/-30/30/ -30/30/0/30/0/-30/0_4/-30/0/30/0/30/-30]$	C12K/R6376

## APPENDIX

Tabulated data of the energy release rate distribution is presented at five points across the width of DCB, ENF and SLB specimens made of unidirectional and  $D\pm 30$  multidirectional layup. This appeared helpful as it was difficult to distinguish between data points on the  $G$  distribution plots for the individual specimens.

TABLE A. NORMALIZED STRAIN ENERGY RELEASE RATE  $G_I / G_{I,beam}$   
FOR DCB SPECIMEN WITH UD24 LAYUP

y/B	d/2h=1.67	d/2h=3.3	d/2h=5.0	d/2h=6.67	d/2h=8.33	d/2h=10.	full 3D
-0.42	0.48046 <sup>1</sup>	0.89624 <sup>1</sup>	0.97704 <sup>1</sup>	0.98897 <sup>1</sup>	0.99069 <sup>1</sup>	0.99094 <sup>1</sup>	0.99253 <sup>1</sup>
	0.50666 <sup>2</sup>	0.91518 <sup>2</sup>	0.97151 <sup>2</sup>	0.97741 <sup>2</sup>	0.97790 <sup>2</sup>	0.97802 <sup>2</sup>	0.97692 <sup>2</sup>
-0.187	0.55314 <sup>1</sup>	1.0129 <sup>1</sup>	1.1016 <sup>1</sup>	1.1146 <sup>1</sup>	1.1165 <sup>1</sup>	1.1167 <sup>1</sup>	1.1162 <sup>1</sup>
	0.58745 <sup>2</sup>	1.0442 <sup>2</sup>	1.1067 <sup>2</sup>	1.1133 <sup>2</sup>	1.1139 <sup>2</sup>	1.1140 <sup>2</sup>	1.1124 <sup>2</sup>
0.0	0.55942 <sup>1</sup>	1.0256 <sup>1</sup>	1.1155 <sup>1</sup>	1.1288 <sup>1</sup>	1.1306 <sup>1</sup>	1.1309 <sup>1</sup>	1.1298 <sup>1</sup>
	0.59422 <sup>2</sup>	1.0569 <sup>2</sup>	1.1203 <sup>2</sup>	1.1272 <sup>2</sup>	1.1279 <sup>2</sup>	1.1281 <sup>2</sup>	1.1265 <sup>2</sup>
0.187	0.55314 <sup>1</sup>	1.0129 <sup>1</sup>	1.1016 <sup>1</sup>	1.1146 <sup>1</sup>	1.1165 <sup>1</sup>	1.1167 <sup>1</sup>	1.1162 <sup>1</sup>
	0.58745 <sup>2</sup>	1.0442 <sup>2</sup>	1.1067 <sup>2</sup>	1.1133 <sup>2</sup>	1.1139 <sup>2</sup>	1.1140 <sup>2</sup>	1.1124 <sup>2</sup>
0.42	0.48046 <sup>1</sup>	0.89624 <sup>1</sup>	0.97704 <sup>1</sup>	0.98897 <sup>1</sup>	0.99069 <sup>1</sup>	0.99094 <sup>1</sup>	0.99253 <sup>1</sup>
	0.50666 <sup>2</sup>	0.91518 <sup>2</sup>	0.97151 <sup>2</sup>	0.97741 <sup>2</sup>	0.97790 <sup>2</sup>	0.97802 <sup>2</sup>	0.97692 <sup>2</sup>

<sup>1</sup> 3D region modeled with twenty noded elements

<sup>2</sup> 3D region modeled with eight noded elements

TABLE B. NORMALIZED STRAIN ENERGY RELEASE RATE  $G_{II} / G_{II,beam}$   
FOR ENF SPECIMEN WITH UD24 LAYUP

y/B	d/2h=1.67	d/2h=3.3	d/2h=5.0	d/2h=6.67	d/2h=8.33	d/2h=10.	full 3D
-0.42	0.98596	1.0330	1.0352	1.0354	1.0354	1.0354	1.0402
-0.187	0.97854	1.0250	1.0270	1.0273	1.0273	1.0273	1.0322
0.0	0.97147	1.0175	1.0194	1.0197	1.0197	1.0197	1.0246
0.187	0.97854	1.0250	1.0270	1.0273	1.0273	1.0273	1.0322
0.42	0.98596	1.0330	1.0352	1.0354	1.0354	1.0354	1.0402

TABLE C. NORMALIZED STRAIN ENERGY RELEASE RATE  $G_{III}/G_{II,beam}$   
FOR ENF SPECIMEN WITH UD24 LAYUP

y/B	d/2h=1.67	d/2h=3.3	d/2h=5.0	d/2h=6.67	d/2h=8.33	d/2h=10.	full 3D
-0.42	0.0064968	0.0064509	0.0064050	0.0064050	0.0064050	0.0064050	0.0066346
-0.187	0.0003444	0.0003444	0.0003444	0.0003444	0.0003444	0.0003444	0.0003673
0.0	0.0	0.0	0.0	0.0	0.0	0.0	0.0
0.187	0.0003444	0.0003444	0.0003444	0.0003444	0.0003444	0.0003444	0.0003673
0.42	0.0064968	0.0064509	0.0064050	0.0064050	0.0064050	0.0064050	0.0066346

TABLE D. STRAIN ENERGY RELEASE RATE  $G_I$  [kJ/m<sup>2</sup>]  
FOR SLB SPECIMEN WITH UD32 LAYUP

y/B	d/2h=1.48	d/2h=2.46	d/2h=3.69	d/2h=4.93	d/2h=6.16	d/2h=7.39	full 3D
-0.436	0.00594	0.01056	0.01243	0.01279	0.01285	0.01286	0.01285
-0.194	0.00696	0.01204	0.01407	0.01447	0.01454	0.01455	0.01454
0.0	0.0693	0.01202	0.01406	0.01446	0.01453	0.01455	0.01453
0.194	0.00696	0.01204	0.01407	0.01447	0.01454	0.01455	0.01454
0.436	0.00594	0.01056	0.01243	0.01279	0.01285	0.01286	0.01285

TABLE E. STRAIN ENERGY RELEASE RATE  $G_{II}$  [kJ/m<sup>2</sup>]  
FOR SLB SPECIMEN WITH UD32 LAYUP

y/B	d/2h=1.48	d/2h=2.46	d/2h=3.69	d/2h=4.93	d/2h=6.16	d/2h=7.39	full 3D
-0.436	0.00832	0.00873	0.00881	0.00882	0.00883	0.00883	0.00884
-0.194	0.00838	0.00880	0.00889	0.00890	0.00890	0.00890	0.00891
0.0	0.00834	0.00876	0.00885	0.00886	0.00886	0.00886	0.00887
0.194	0.00838	0.00880	0.00889	0.00890	0.00890	0.00890	0.00891
0.436	0.00832	0.00873	0.00881	0.00882	0.00883	0.00883	0.00884

TABLE F. STRAIN ENERGY RELEASE RATE  $G_{III}$  [kJ/m<sup>2</sup>]  
FOR SLB SPECIMEN WITH UD32 LAYUP

y/B	d/2h=1.48	d/2h=2.46	d/2h=3.69	d/2h=4.93	d/2h=6.16	d/2h=7.39	full 3D
-0.436	0.00011	0.00011	0.00011	0.00011	0.00011	0.00011	0.00011
-0.194	0.00001	0.00001	0.00001	0.00001	0.00001	0.00001	0.00001
0.0	0.0	0.0	0.0	0.0	0.0	0.0	0.0
0.194	0.00001	0.00001	0.00001	0.00001	0.00001	0.00001	0.00001
0.436	0.00011	0.00011	0.00011	0.00011	0.00011	0.00011	0.00011

TABLE G. STRAIN ENERGY RELEASE RATE  $G_I$  [kJ/m<sup>2</sup>]  
FOR DCB SPECIMEN WITH D±30 LAYUP

y/B	d/2h=0.74	d/2h=2.46	d/2h=3.69	d/2h=4.93	d/2h=6.16	d/2h=7.39	full 3D
-0.431	0.00010	0.00307	0.00337	0.00342	0.00343	0.00344	0.00350
-0.253	0.00205	0.00992	0.01046	0.01053	0.01055	0.01055	0.01043
0.0	0.00225	0.01104	0.01165	0.01173	0.01173	0.01172	0.01159
0.253	0.00205	0.00992	0.01046	0.01053	0.01055	0.01055	0.01043
0.431	0.00010	0.00307	0.00337	0.00342	0.00343	0.00344	0.00350

TABLE H. STRAIN ENERGY RELEASE RATE  $G_{II}$  [kJ/m<sup>2</sup>]  
FOR ENF SPECIMEN WITH D±30 LAYUP

y/B	d/2h=0.74	d/2h=2.46	d/2h=3.69	d/2h=4.93	d/2h=6.16	d/2h=7.39	full 3D
-0.431	0.00767	0.01060	0.01046	0.01058	0.01067	0.01075	0.01099
-0.253	0.00787	0.01158	0.01160	0.01153	0.01146	0.01141	0.01137
0.0	0.00749	0.01121	0.01132	0.01134	0.01131	0.01127	0.01140
0.253	0.00787	0.01158	0.01160	0.01153	0.01146	0.01141	0.01137
0.431	0.00767	0.01060	0.01046	0.01057	0.01066	0.01074	0.01098

TABLE I. STRAIN ENERGY RELEASE RATE  $G_{III}$  [kJ/m<sup>2</sup>]  
FOR ENF SPECIMEN WITH D±30 LAYUP

y/B	d/2h=0.74	d/2h=2.46	d/2h=3.69	d/2h=4.93	d/2h=6.16	d/2h=7.39	full 3D
-0.431	0.00190	0.00234	0.00252	0.00258	0.00265	0.00270	0.00279
-0.253	0.00013	0.00014	0.00015	0.00017	0.00019	0.00021	0.00021
0.0	0.0	0.0	0.0	0.0	0.0	0.0	0.0
0.253	0.00013	0.00014	0.00015	0.00018	0.00020	0.00021	0.00021
0.431	0.00190	0.00234	0.00253	0.00259	0.00265	0.00271	0.00279

TABLE J. STRAIN ENERGY RELEASE RATE  $G_I$  [kJ/m<sup>2</sup>]  
FOR SLB SPECIMEN WITH D±30 LAYUP

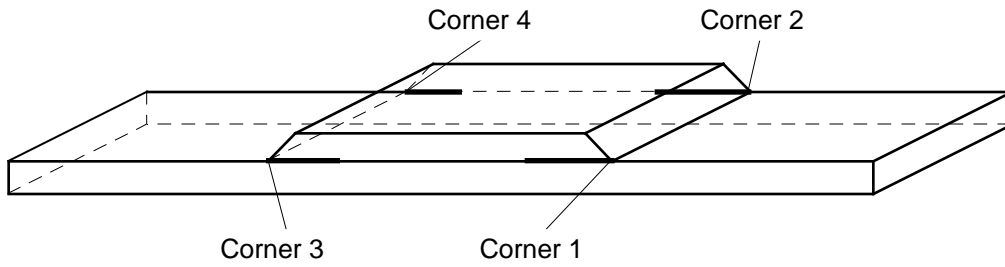
y/B	d/2h=0.74	d/2h=2.46	d/2h=3.69	d/2h=4.93	d/2h=6.16	d/2h=7.39	full 3D
-0.431	0.00076	0.00931	0.00997	0.01003	0.01001	0.01000	0.01000
-0.253	0.0045	0.02171	0.02279	0.02290	0.02290	0.02290	0.02263
0.0	0.0043	0.02231	0.02366	0.02386	0.02390	0.02391	0.02359
0.253	0.00487	0.02313	0.02451	0.02478	0.02487	0.02491	0.02448
0.431	0.00159	0.01313	0.01415	0.01432	0.01434	0.01433	0.01415

TABLE K. STRAIN ENERGY RELEASE RATE  $G_{II}$  [kJ/m<sup>2</sup>]  
FOR SLB SPECIMEN WITH D±30 LAYUP

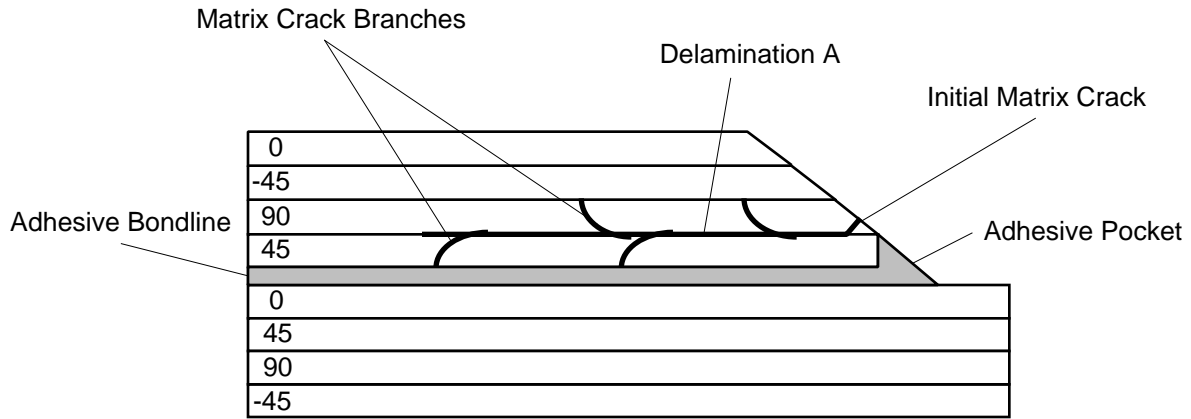
y/B	d/2h=0.74	d/2h=2.46	d/2h=3.69	d/2h=4.93	d/2h=6.16	d/2h=7.39	full 3D
-0.431	0.00898	0.01221	0.01192	0.01204	0.01212	0.01219	0.01248
-0.253	0.00910	0.01336	0.01333	0.01321	0.01309	0.01303	0.01299
0.0	0.00868	0.01297	0.01310	0.01313	0.01311	0.01307	0.01279
0.253	0.00917	0.01352	0.01360	0.01356	0.01349	0.01345	0.01339
0.431	0.00911	0.01268	0.01261	0.01274	0.01286	0.01296	0.01311

TABLE L. STRAIN ENERGY RELEASE RATE  $G_{III}$  [kJ/m<sup>2</sup>]  
 FOR SLB SPECIMEN WITH D±30 LAYUP

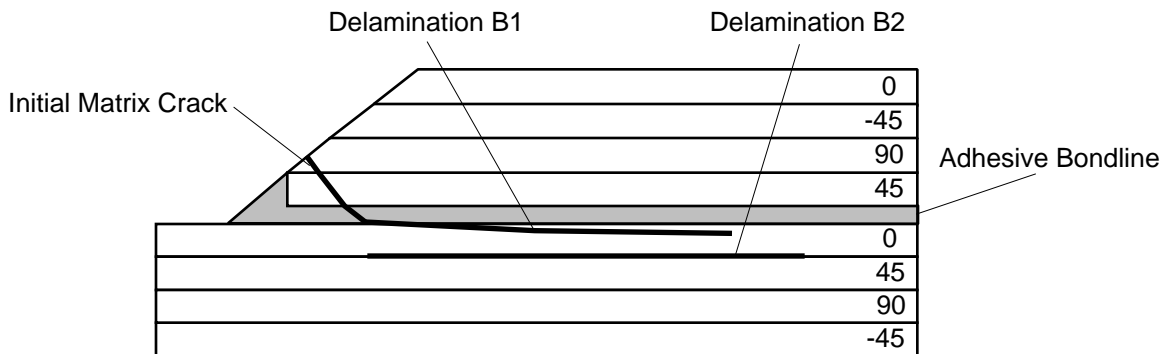
y/B	d/2h=0.74	d/2h=2.46	d/2h=3.69	d/2h=4.93	d/2h=6.16	d/2h=7.39	full 3D
-0.431	0.00303	0.00439	0.00470	0.00476	0.00485	0.00492	0.00487
-0.253	0.00050	0.00085	0.00092	0.00098	0.00104	0.00108	0.00099
0.0	0.00005	0.00018	0.00020	0.00020	0.00020	0.00020	0.00019
0.253	0.00005	0.0	0.0	0.0	0.00001	0.00001	0.00001
0.431	0.00206	0.00204	0.00221	0.00228	0.00236	0.00242	0.00247



(a) Specimen with crack locations.



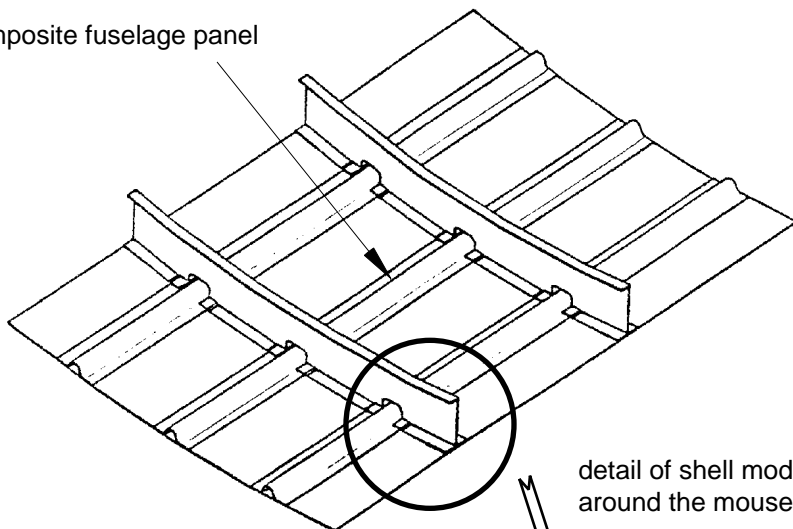
(b) Corners 1 and 4



(c) Corners 2 and 3

Figure 1. Typical damage patterns observed in skin/stringer specimens [23]

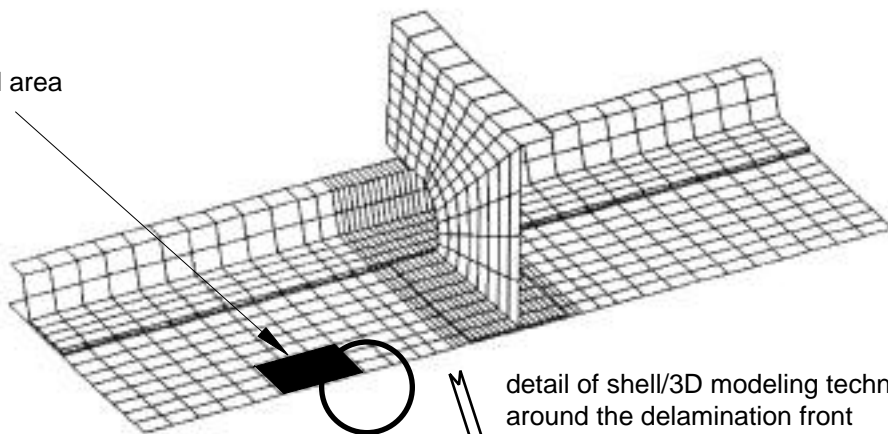
composite fuselage panel



detail of shell model  
around the mousehole



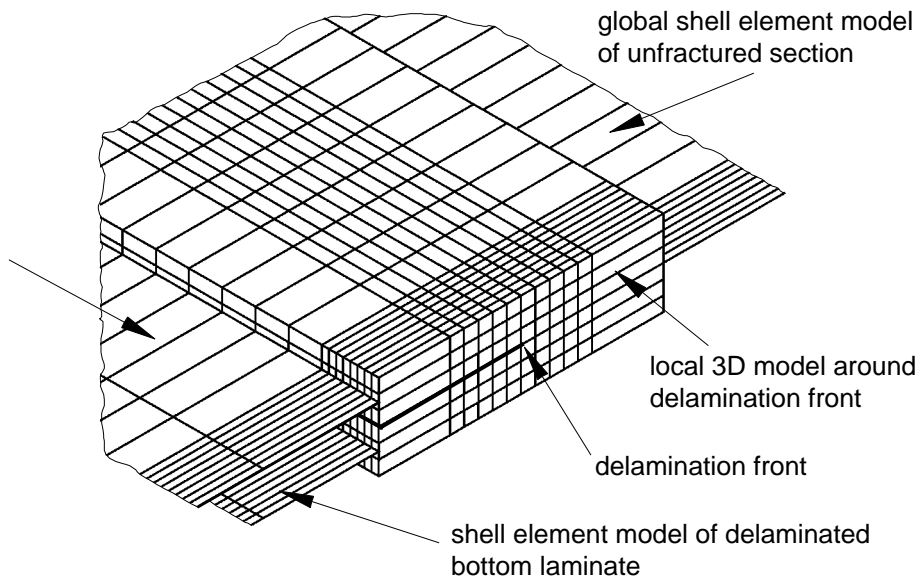
delaminated area



detail of shell/3D modeling technique  
around the delamination front



shell element model of  
delaminated top laminate



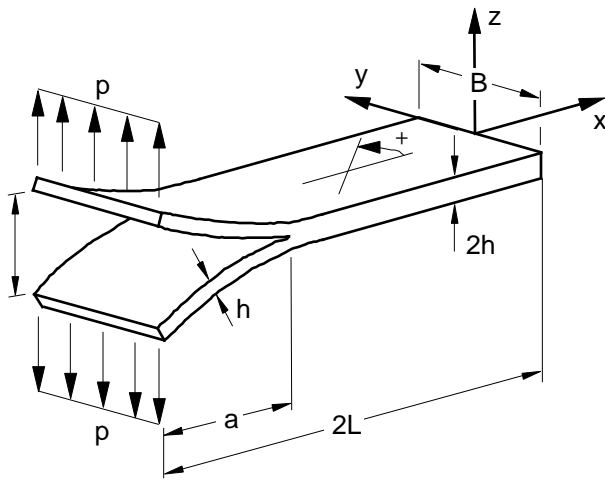
global shell element model  
of unfractured section

local 3D model around  
delamination front

delamination front

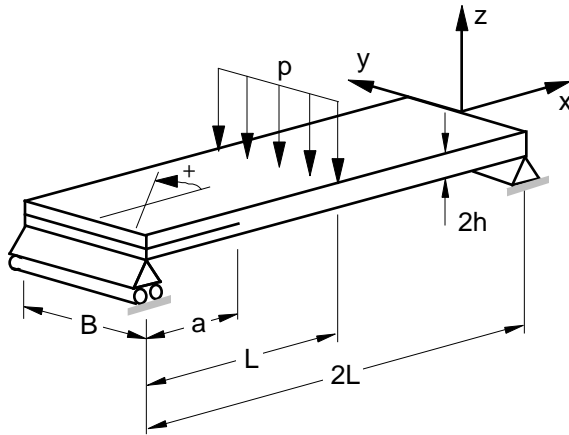
shell element model of delaminated  
bottom laminate

Figure 2. Application of shell/3D modeling technique to large built-up structures.



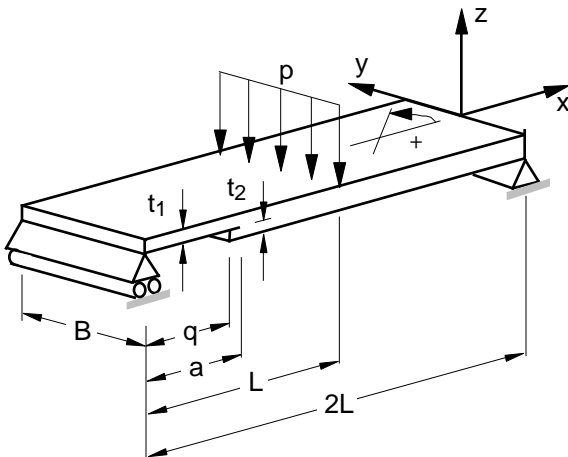
	layup UD24	layup D±30
B	25.0 mm	25.4 mm
2h	3.0 mm	4.06 mm
2L	150.0 mm	150.0 mm
a	111.5 mm	57.2 mm
P	12.66 N	10.0 N

(a) Double Cantilever Beam Specimen (DCB)



	layup UD24	layup D±30
B	25.0 mm	25.5 mm
2h	3.0 mm	4.06 mm
2L	150.0 mm	127.0 mm
a	30.0 mm	31.8 mm
P	503.0 N	100.0 N

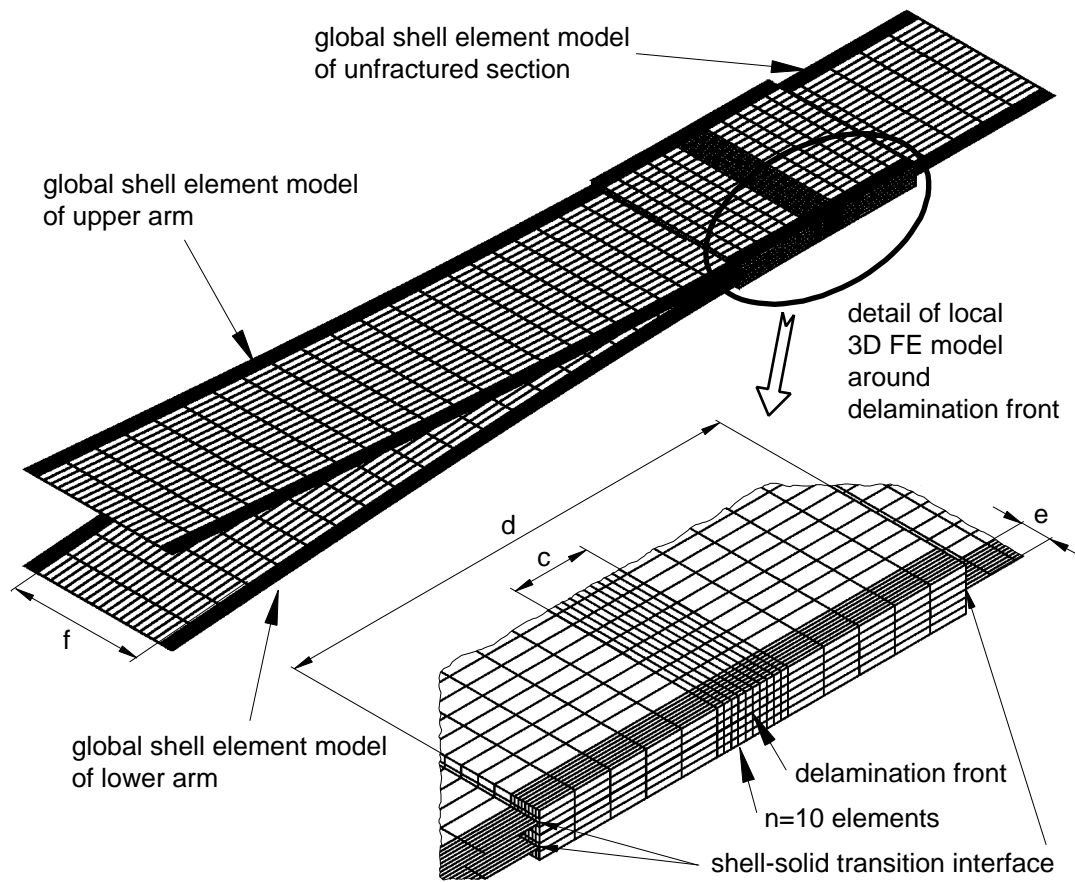
(b) End Notched Flexure Specimen (ENF)



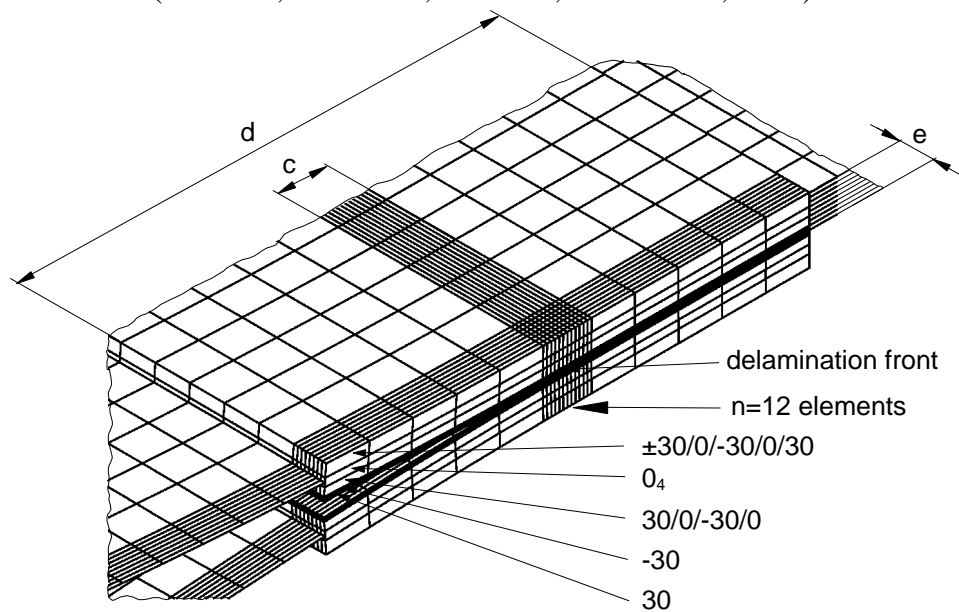
	layup UD32	layup D±30
B	25.0 mm	25.4 mm
t <sub>1</sub>	2.03 mm	2.03 mm
t <sub>2</sub>	2.03 mm	2.03 mm
2L	177.8 mm	177.8 mm
a	34.3 mm	34.3 mm
P	100.0 N	100.0 N
q	portion of lower arm removed to ensure entire support force is transmitted to upper arm [25]	

(c) Single Leg Bending Specimen (SLB)

Figure 3. Specimen configurations.



(a) FE model and detail around delamination front for specimen with UD24 layup  
( $c=5$  mm,  $d=30$  mm,  $e=2$  mm,  $f=21.0$  mm,  $n=10$ )



(b) Detail around delamination front for specimen with D±30 layup  
( $c=5$  mm,  $d=30$  mm,  $e=2$  mm,  $f=21.0$  mm,  $n=12$ )

Figure 4. Shell/3D finite element model of a DCB specimen. .

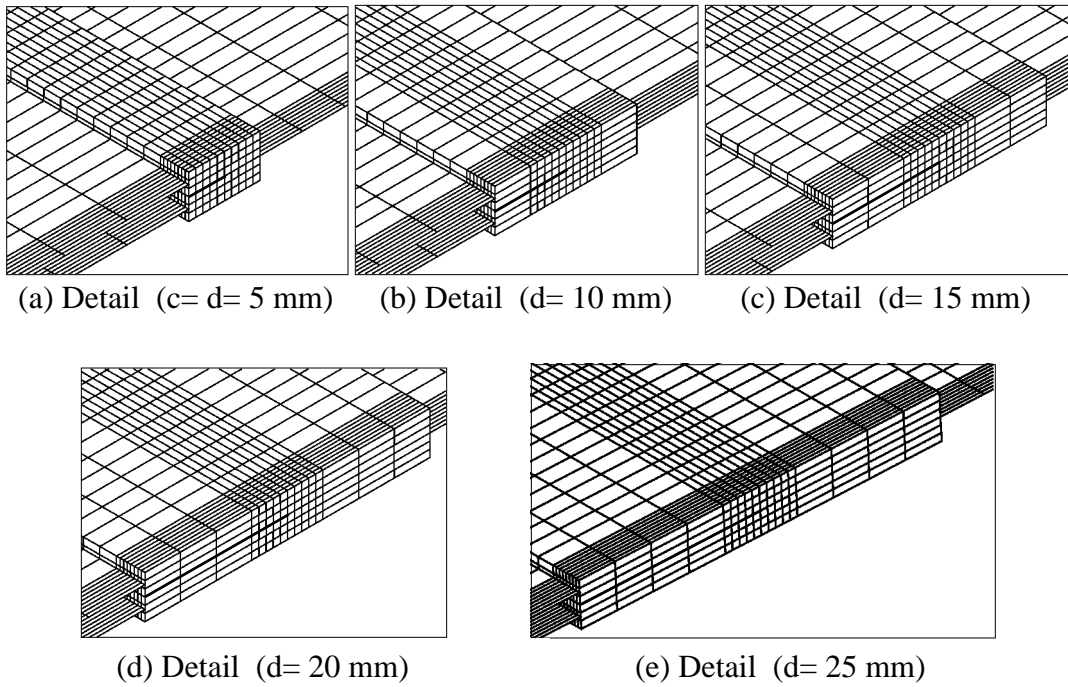


Figure 5. Shell/3D Finite element model of a DCB Specimen with UD24 layup.

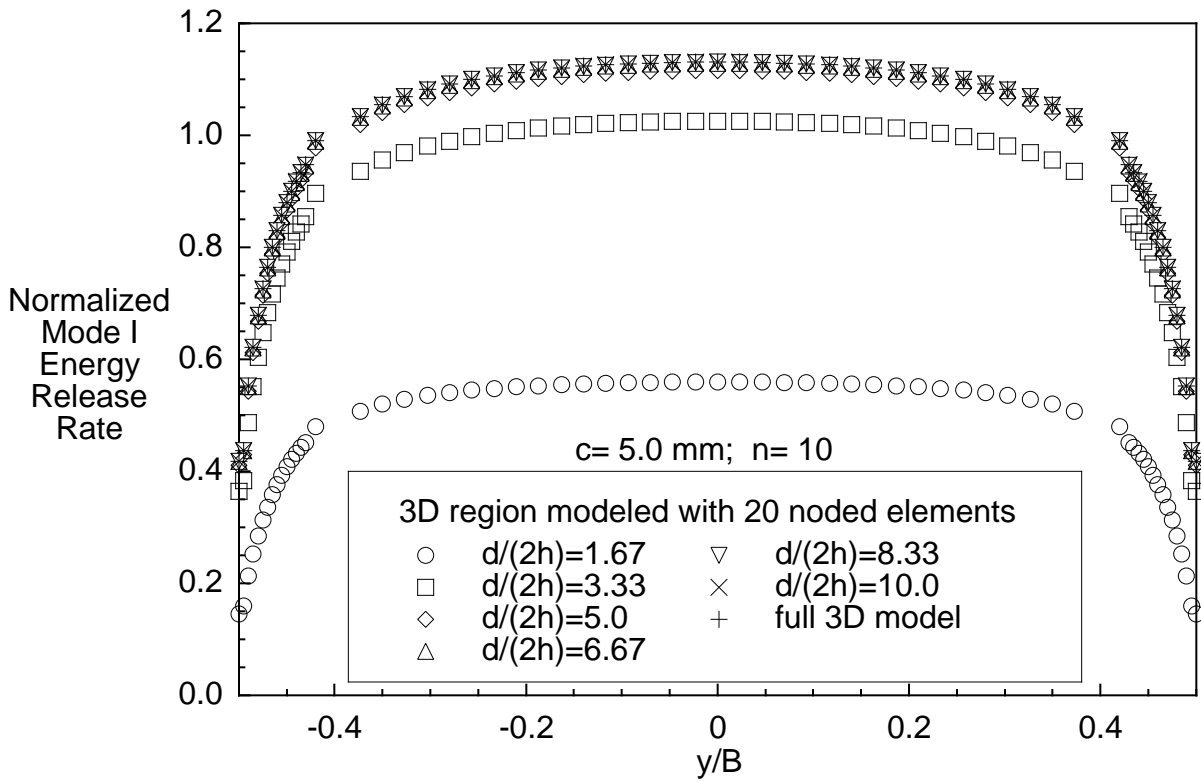


Figure 6. Strain energy release rate distribution across the width of a DCB specimen with UD24 layup modeled with 20 noded elements.

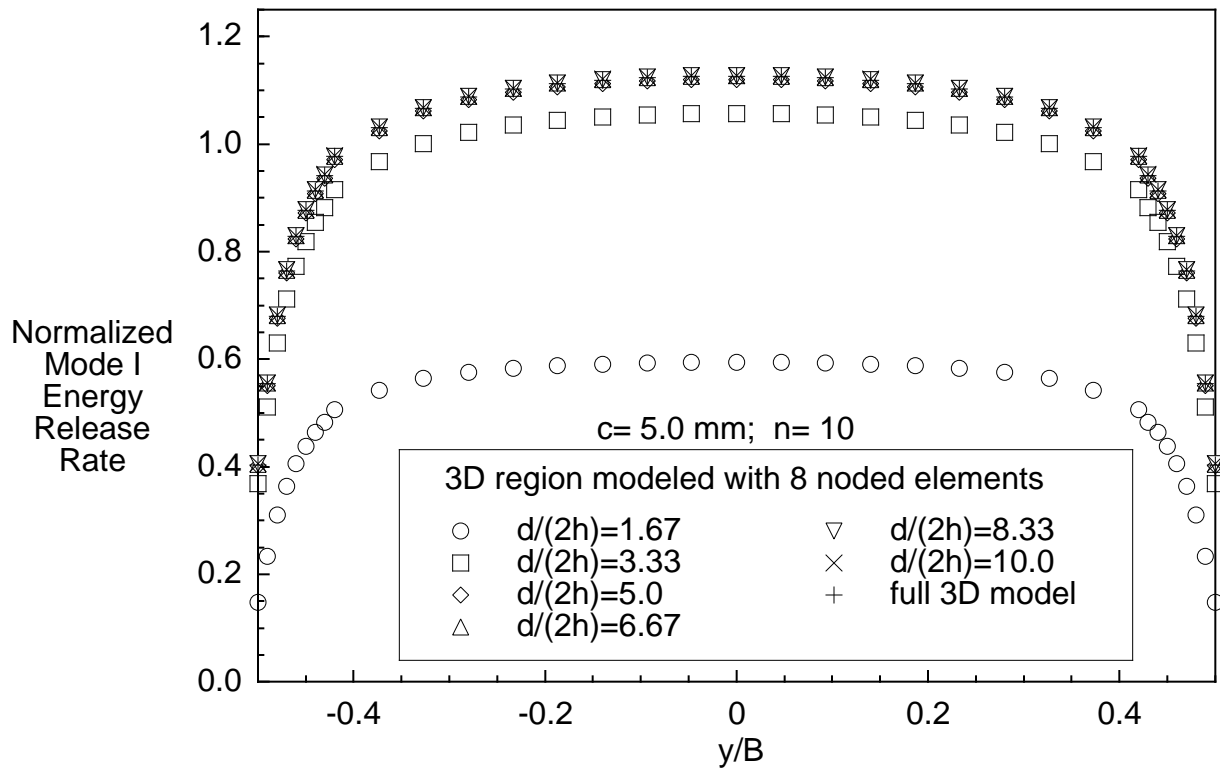


Figure 7. Strain energy release rate distribution across the width of a DCB specimen with UD24 layup modeled with 8 noded elements.

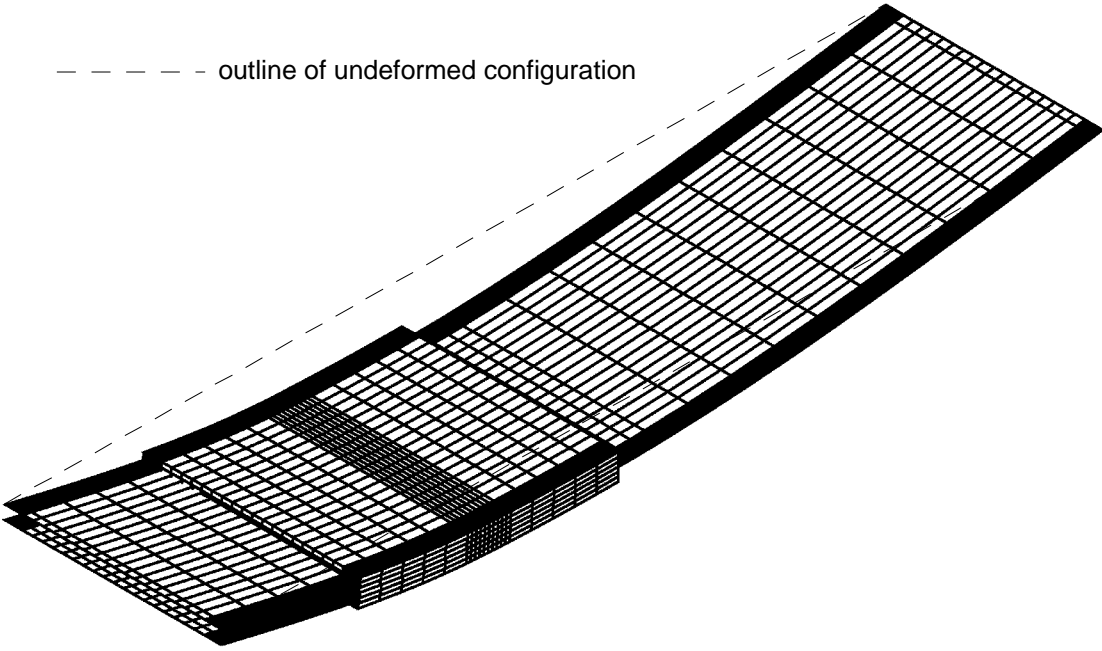


Figure 8. Shell/3Dfinite element model of an ENF specimen with UD24 layup (c= 5 mm, n= 10, d= 30 mm)

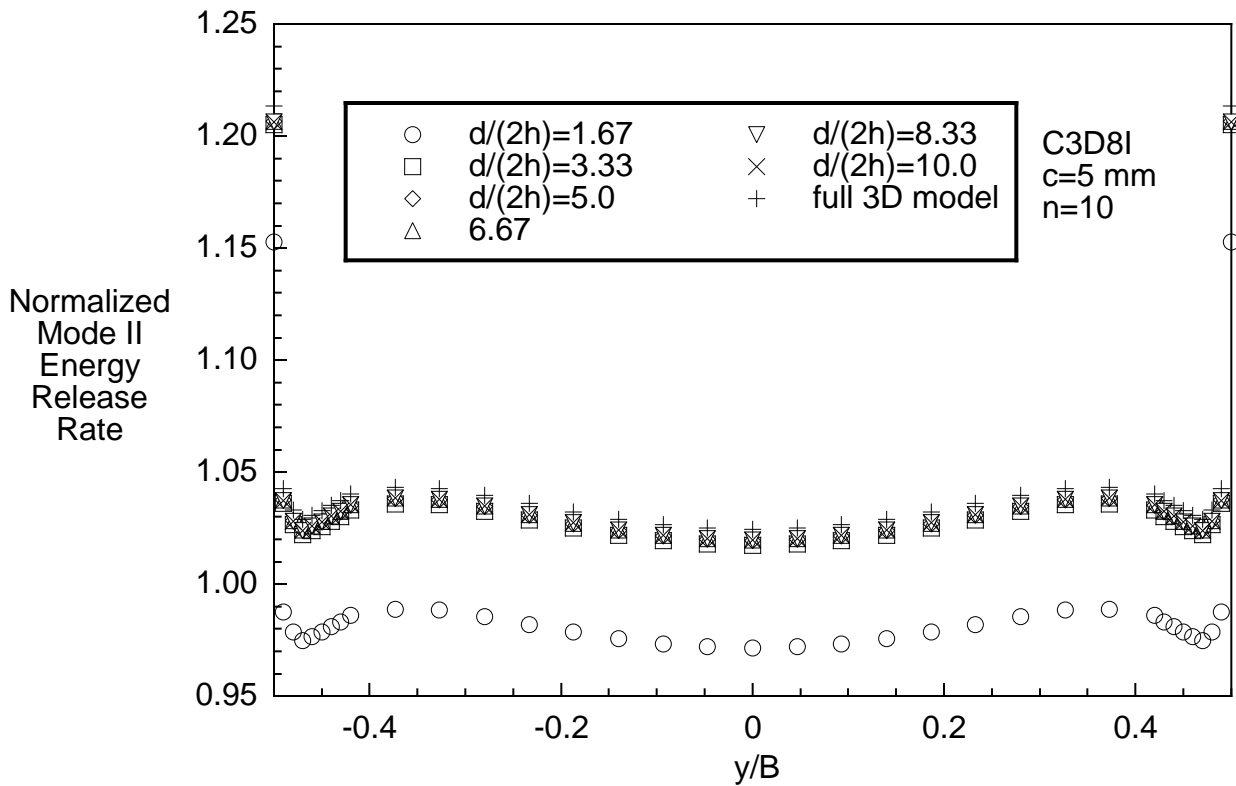


Figure 9. Mode II strain energy release rate distribution across the width of an ENF specimen with UD24 layup calculated using the shell/3D modeling technique

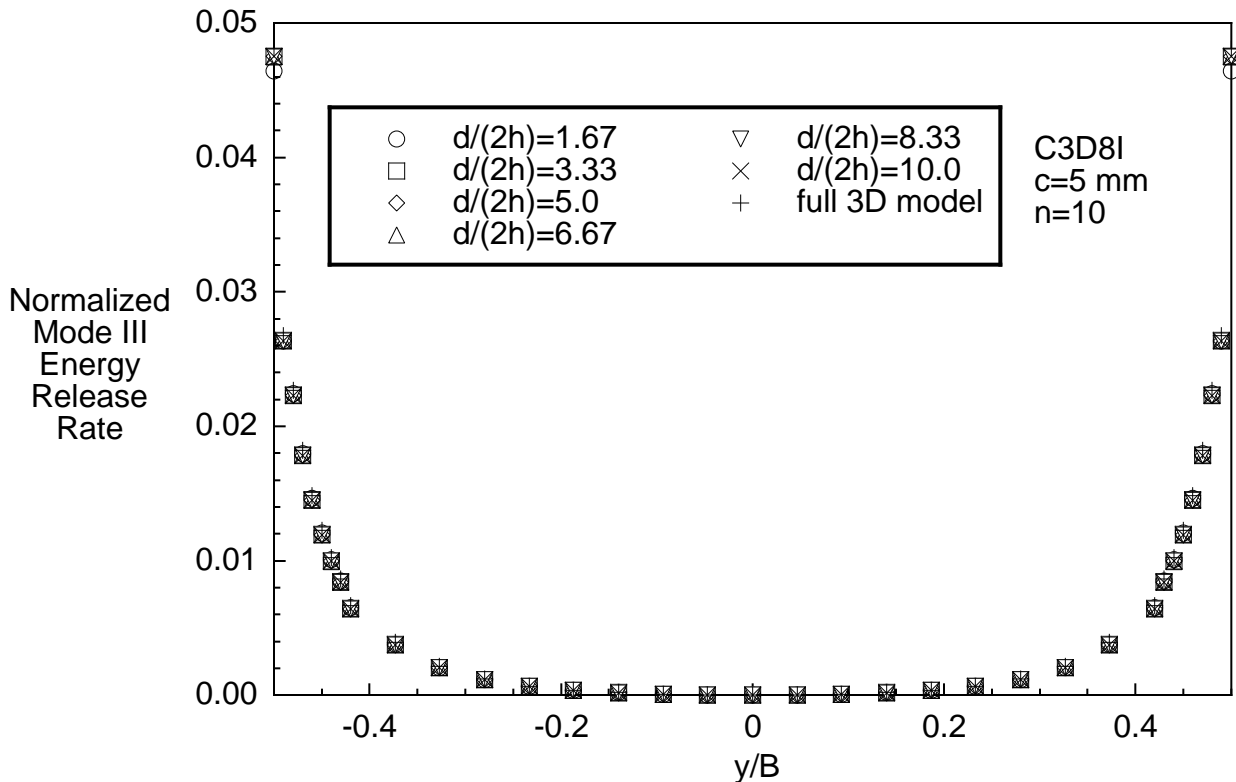


Figure 10. Mode III strain energy release rate distribution across the width of an ENF specimen with UD24 layup calculated using the shell/3D modeling technique.

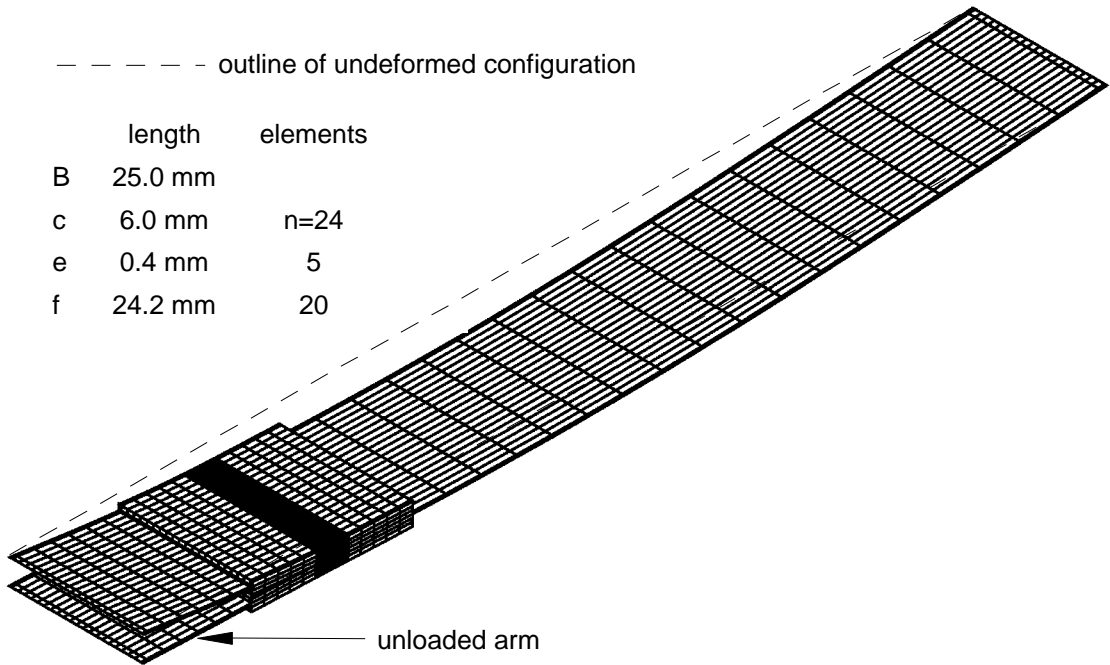


Figure 11. Shell/3Dfinite element model of a SLB Specimen with UD32 layup  
(c= 6mm, n= 24, d= 30 mm)

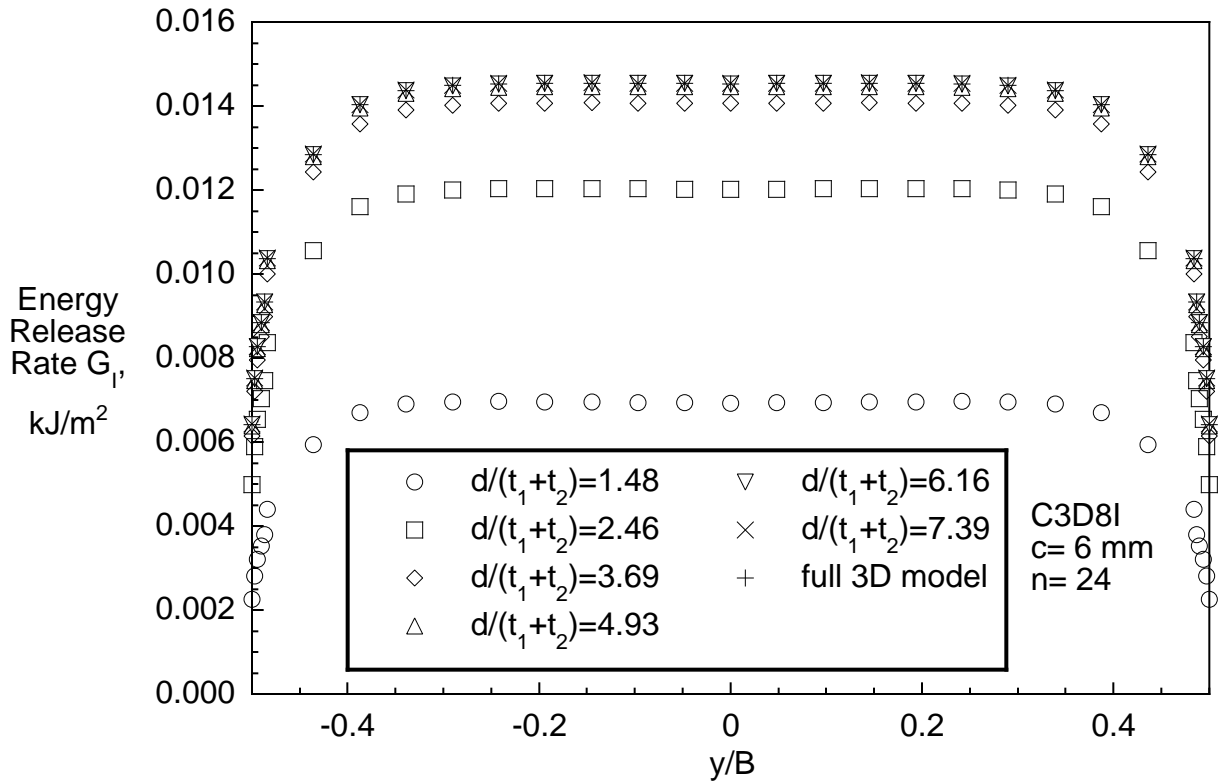


Figure 12. Mode I strain energy release rate distribution across the width of a SLB specimen with UD32 layup calculated using the shell/3D modeling technique

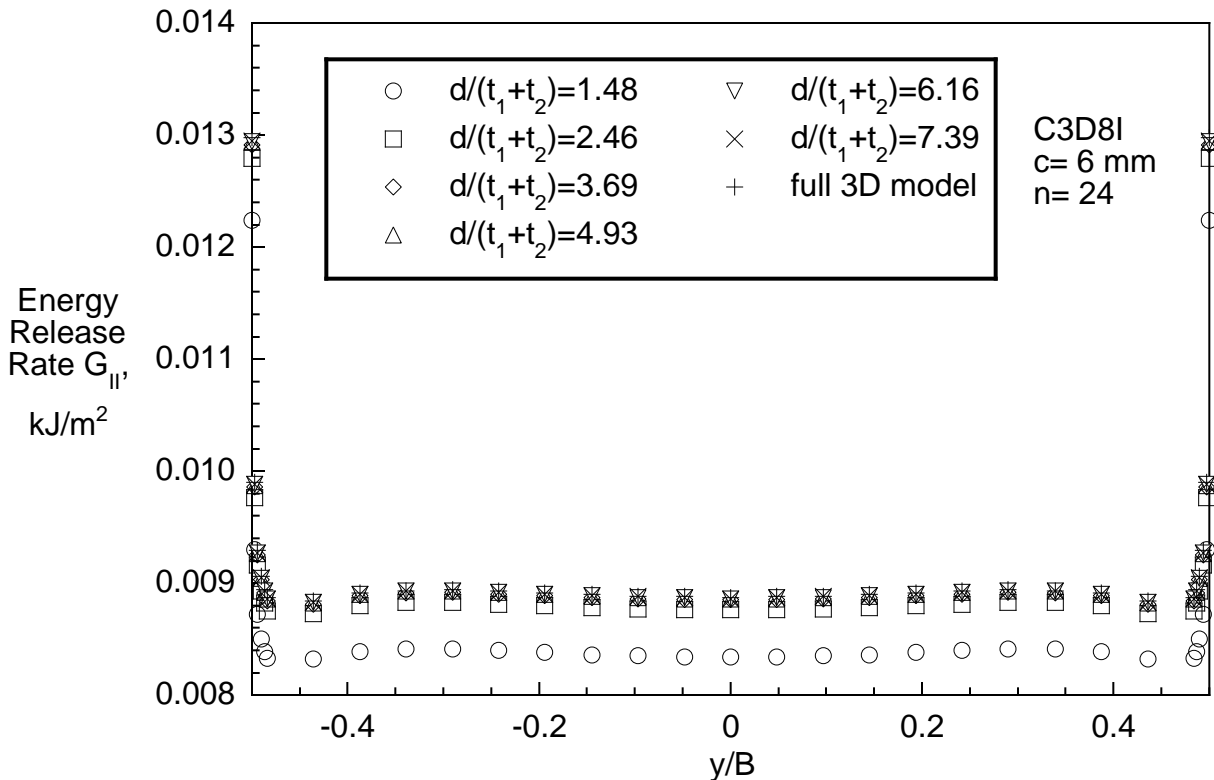


Figure 13. Mode II strain energy release rate distribution across the width of a SLB specimen with UD32 layup calculated using the shell/3D modeling technique

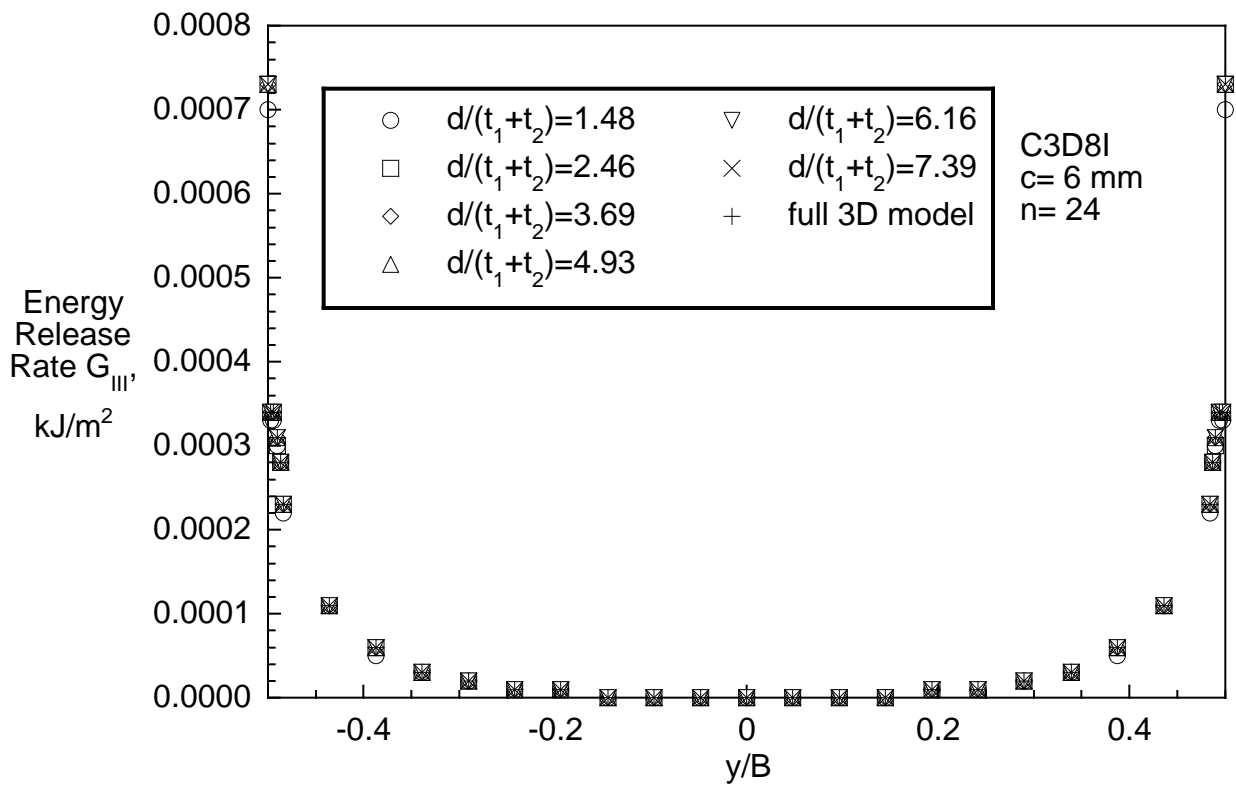


Figure 14. Mode III strain energy release rate distribution across the width of a SLB specimen with UD32 layup calculated using the shell/3D modeling technique

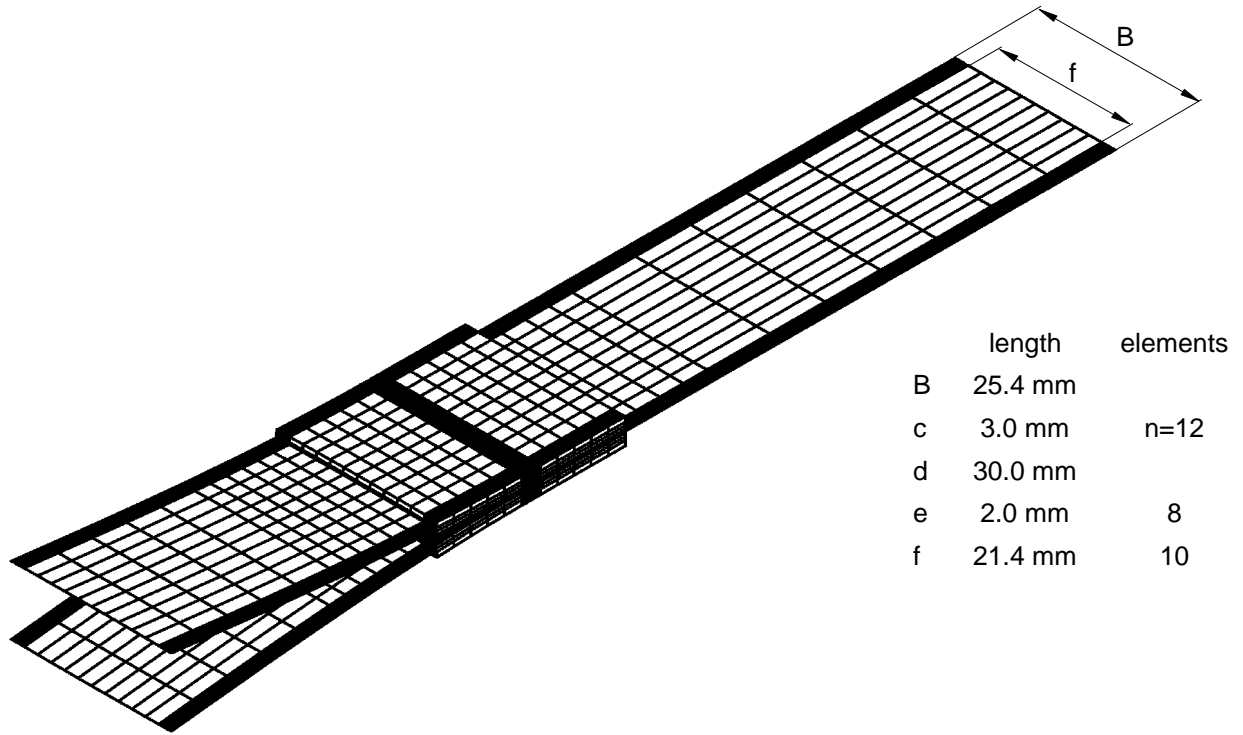


Figure 15. Shell/3Dfinite element model of a DCB specimen with D±30 layup

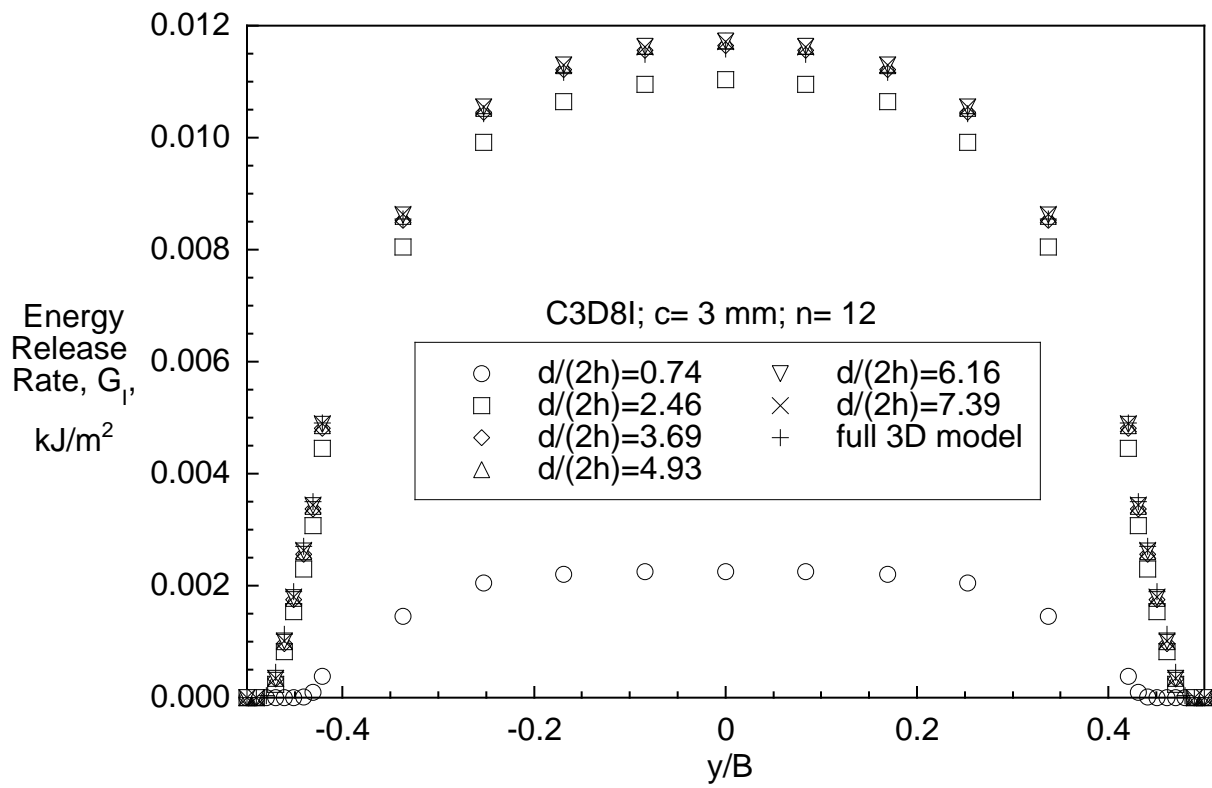


Figure 16. Mode I strain energy release rate distribution across the width of a DCB specimen with  $D_{\pm 30}$  layup calculated using the shell/3D modeling technique

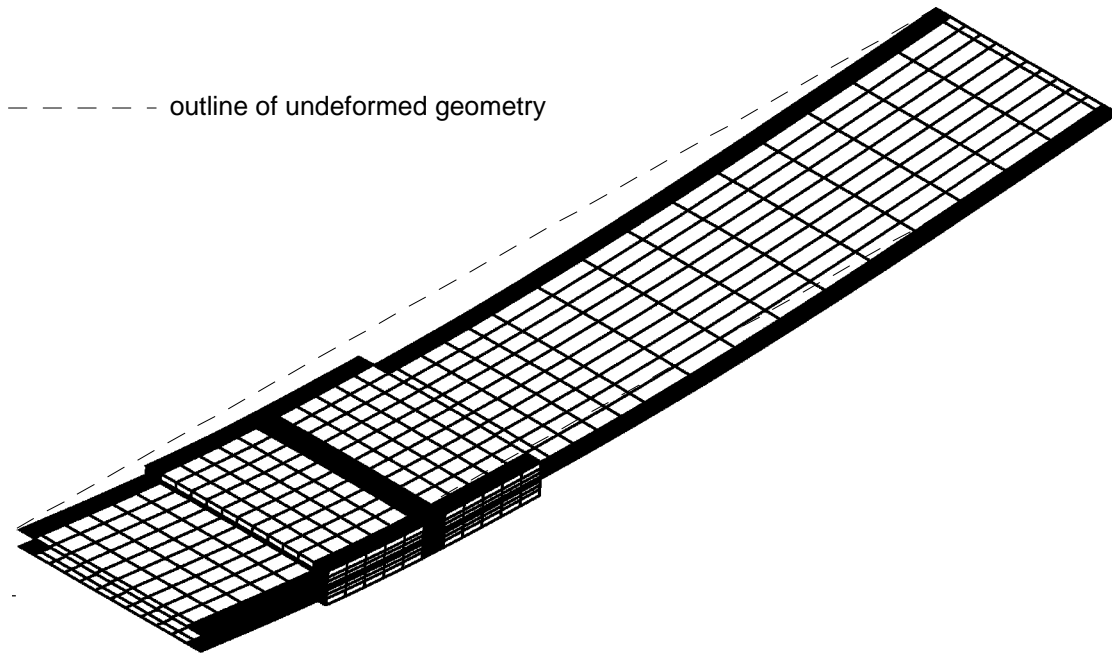


Figure 17. Shell/3Dfinite element model of an ENF specimen with  $D\pm 30$  layup  
( $c=3$  mm,  $n=12$ ,  $d=30$  mm)

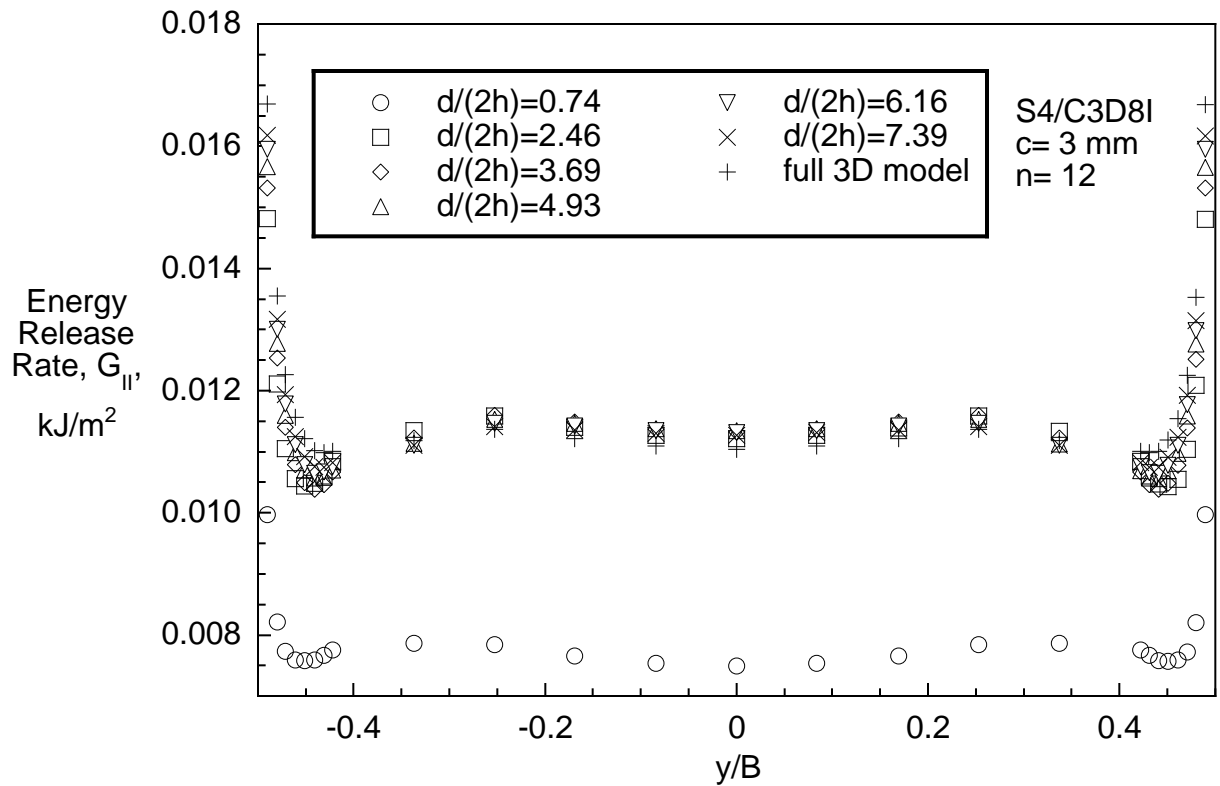


Figure 18. Mode II strain energy release rate distribution across the width of an ENF specimen with D±30 layup calculated using the shell/3D modeling technique

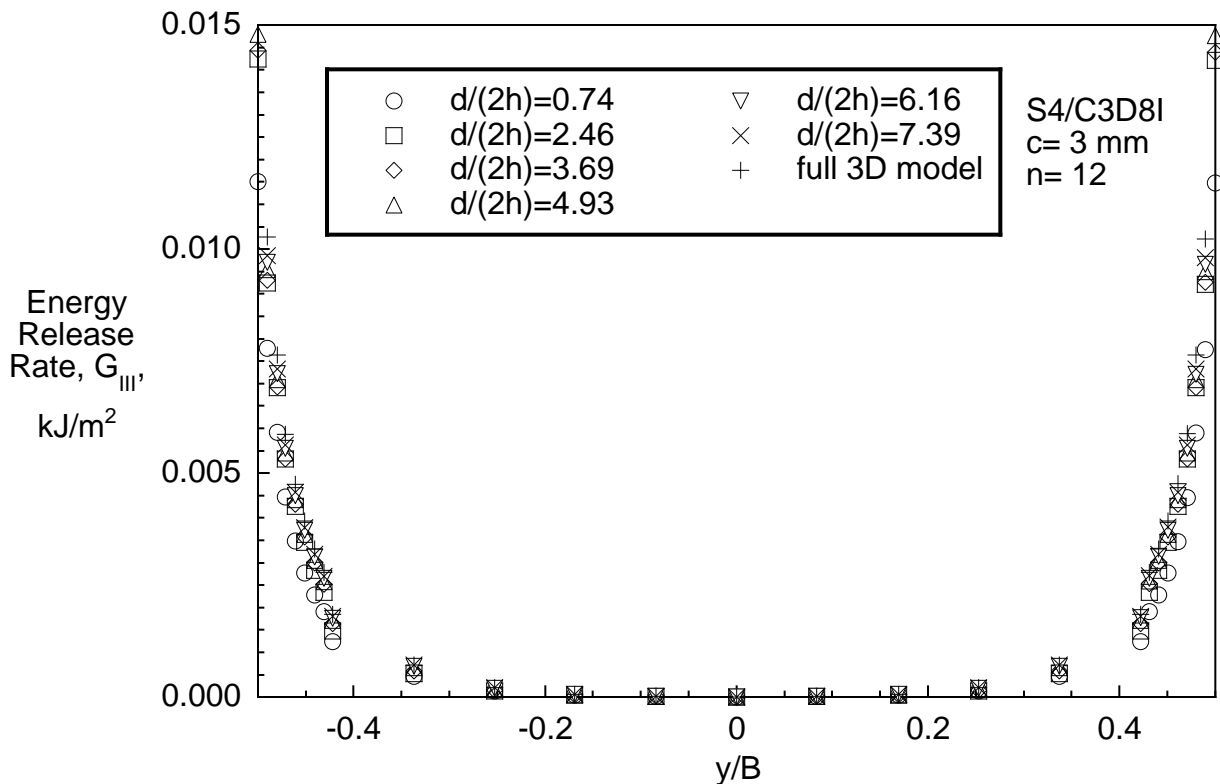


Figure 19. Mode III strain energy release rate distribution across the width of an ENF specimen with D±30 layup calculated using the shell/3D modeling technique

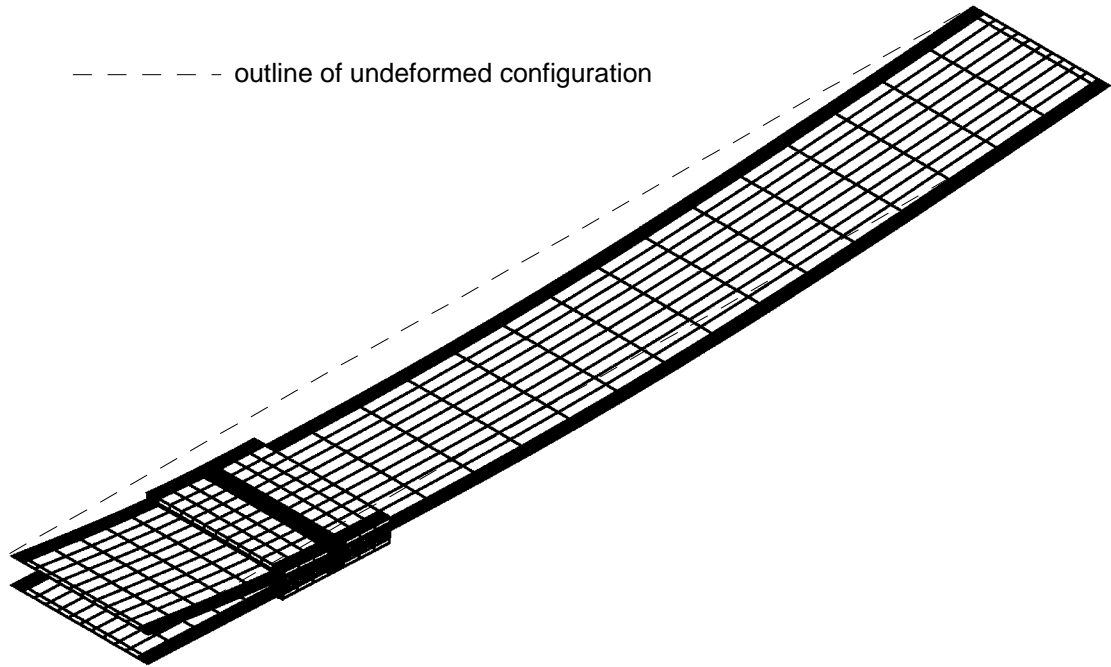


Figure 20. Shell/3D finite element model of a SLB specimen with  $D_{\pm 30}$  layup  
( $c = 3$  mm,  $n = 12$ ,  $d = 20$  mm)

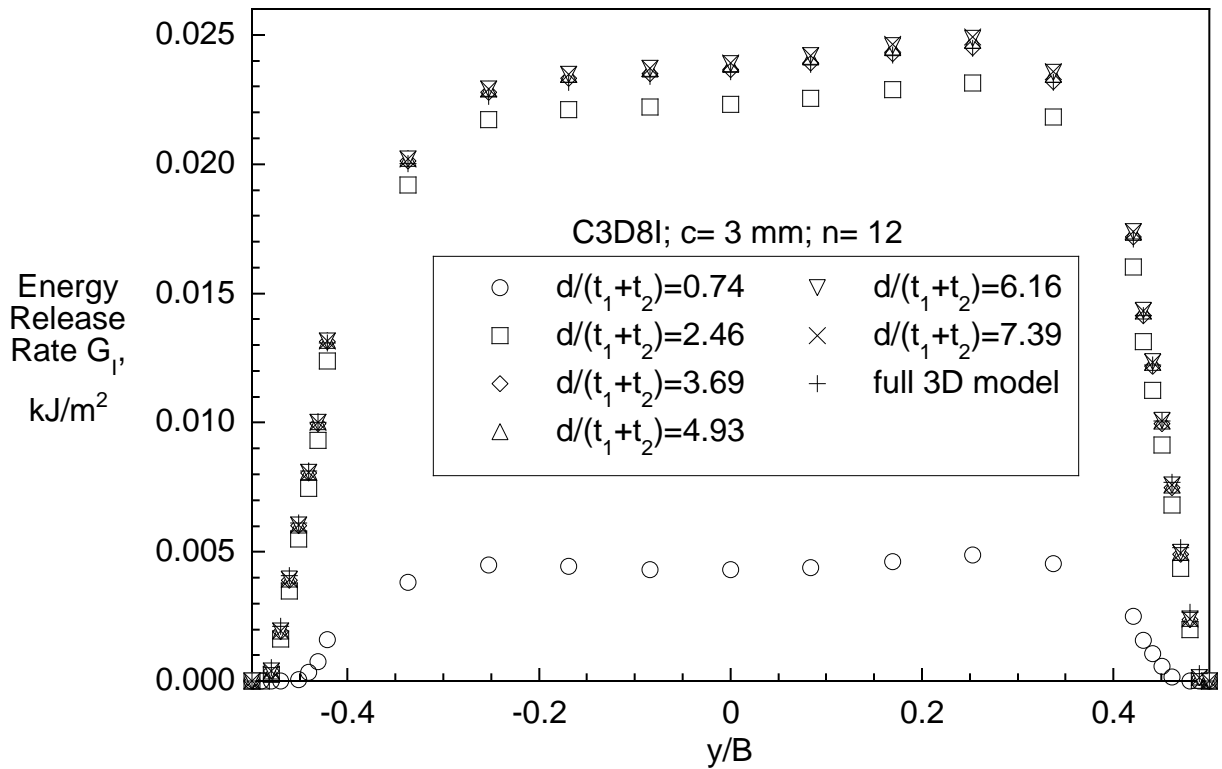


Figure 21. Mode I strain energy release rate distribution across the width of a SLB specimen with  $D\pm 30$  layup calculated using the shell/3D modeling technique

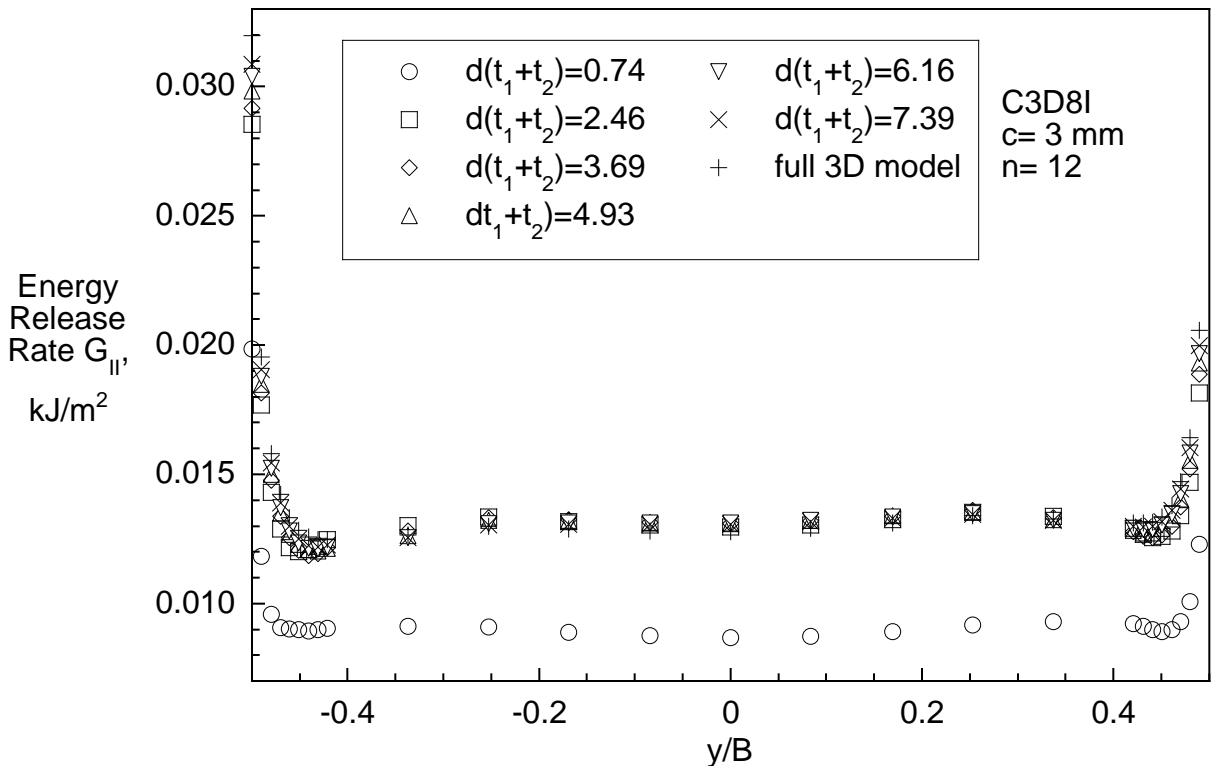


Figure 22. Mode II strain energy release rate distribution across the width of a SLB specimen with  $D\pm 30$  layup calculated using the shell/3D modeling technique

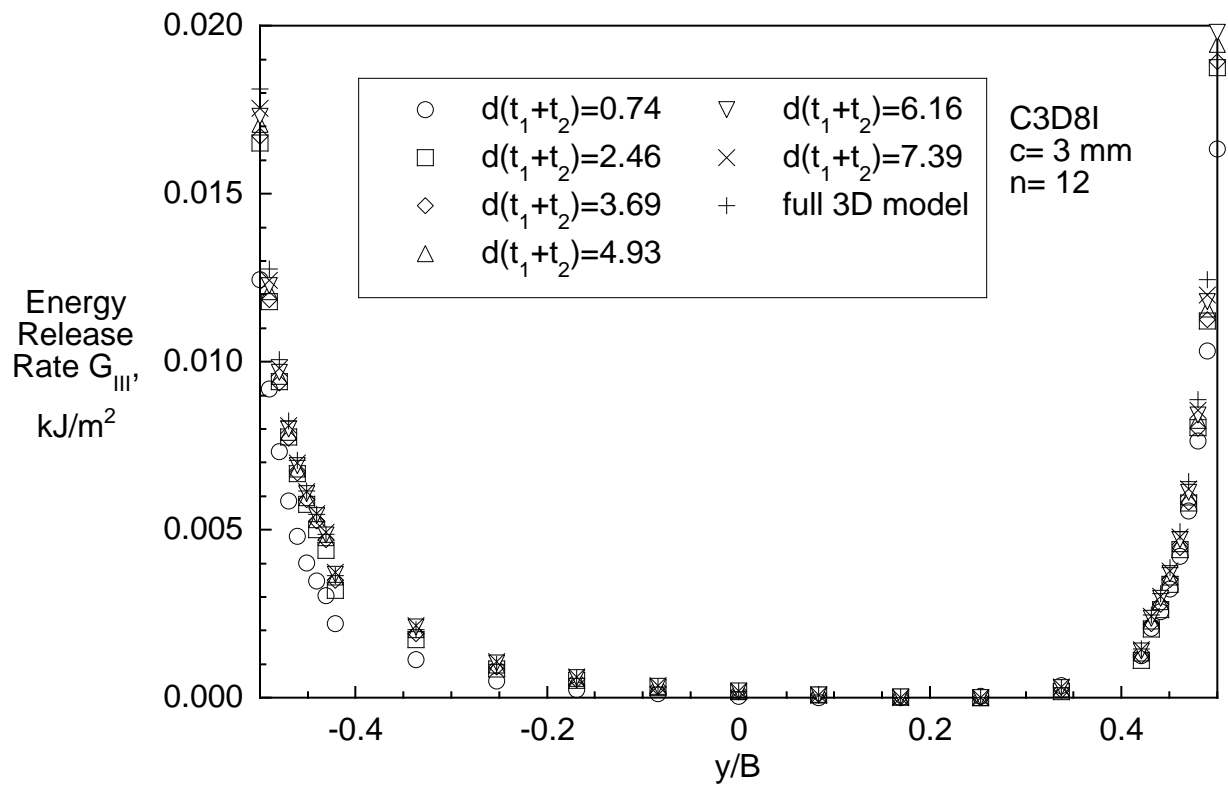


Figure 23. Mode III strain energy release rate distribution across the width of a SLB specimen with D±30 layup calculated using the shell/3D modeling technique